PHOTOGRAPH THIS SHEET

AD-A225 415

DTIC ACCESSION NUMBER

LEVEL

1

INVENTORY

WRDC-TR-90-2084

DOCUMENT IDENTIFICATION

SEPT 90

DISTRIBUTION STATEMENT A

Approved for public release;
Distribution Unlimited

DISTRIBUTION STATEMENT

| ACCESSION FOR | | |
|---|---|---|
| NTIS | GRA&I | ☒ |
| DTIC | TRAC | ☐ |
| UNANNOUNCED | | ☐ |
| JUSTIFICATION | | |
| | | |
| | | |
| | | |
| BY | | |
| DISTRIBUTION/ | | |
| AVAILABILITY CODES | | |
| DISTRIBUTION | AVAILABILITY AND/OR SPECIAL | |
| A-1 | | |

DISTRIBUTION STAMP

DTIC
ELECTE
AUG 20 1990
S E D

DATE ACCESSIONED

QUALITY INSPECTED 4

DATE RETURNED

90 08 15 134

DATE RECEIVED IN DTIC

REGISTERED OR CERTIFIED NUMBER

PHOTOGRAPH THIS SHEET AND RETURN TO DTIC-FDAC

DTIC FORM 70A APR 87

DOCUMENT PROCESSING SHEET

PREVIOUS EDITIONS MAY BE USED UNTIL STOCK IS EXHAUSTED

AD-A225 415

WRDC-TR-90-2084

# DEVELOPMENT OF A MATHEMATICAL CODE TO PREDICT THERMAL DEGRADATION OF FUEL AND DEPOSIT FORMATION IN A FUEL SYSTEM

Suresh Menon

Flow Research, Inc.
21414 - 68th Avenue South
Kent, WA 98032

September 1990

Final Report for Period August 1989 - April 1990

Approved for Public Release; Distribution Unlimited

AERO PROPULSION AND POWER LABORATORY
WRIGHT RESEARCH AND DEVELOPMENT CENTER
AIR FORCE SYSTEMS COMMAND
WRIGHT-PATTERSON AIR FORCE BASE, OHIO 45433-6563

90 134

NOTICE

When Government drawings, specifications, or other data are used for any purpose other that in connection with a definitely Government related procurement, the United States Government incurs no responsibility nor any obligation whatsoever. The fact that the government may have formulated, or in any way supplied the said drawings, specifications, or other data, is not to be regarded by implication or otherwise in any manner construed, as licensing the holder or any other person or corporation, or a conveying any rights or permission to manufacture, use, or sell any patented invention that may in any way be related thereto.

This report is releasable to the National Technical Information Service (NTIS). At NTIS, it will be available to the general public, including foreign nations.

This technical report has been reviewed and is approved for publication.

JEFFREY A. PEARCE, Capt, USAF
Fuels Branch
Fuels and Lubrication Division
Aero Propulsion and Power Laboratory

CHARLES L. DELANEY, Chief
Fuels Branch
Fuels and Lubrication Division
Aero Propulsion and Power Laboratory

FOR THE COMMANDER

BENITO P. BOTTERI, Chief
Fuels and Lubrication Division
Aero Propulsion and Power Laboratory

If your address has changed, if you wish to be removed from our mailing list, or if the addressee is no longer employed by your organization, please notify WRDC/POSF, Wright-Patterson AFB, Ohio 45433-6563 to help us maintain a current mailing list.

Copies of this report should not be returned unless return is required by security considerations, contractual obligations, or notice on a specific document.

UNCLASSIFIED
SECURITY CLASSIFICATION OF THIS PAGE

# REPORT DOCUMENTATION PAGE

Form Approved
OMB No 0704-0188

| | |
|---|---|
| 1a. REPORT SECURITY CLASSIFICATION<br>UNCLASSIFIED | 1b. RESTRICTIVE MARKINGS |
| 2a. SECURITY CLASSIFICATION AUTHORITY | 3. DISTRIBUTION / AVAILABILITY OF REPORT<br>Approved for public release; distribution unlimited |
| 2b. DECLASSIFICATION / DOWNGRADING SCHEDULE | |
| 4. PERFORMING ORGANIZATION REPORT NUMBER(S)<br>Flow Technical Report No. 502 | 5. MONITORING ORGANIZATION REPORT NUMBER(S)<br>WRDC-TR-90-2084 |
| 6a. NAME OF PERFORMING ORGANIZATION<br>Flow Research, Inc.<br>6b. OFFICE SYMBOL (If applicable) | 7a. NAME OF MONITORING ORGANIZATION<br>Aero Propulsion & Power Laboratory (POSF)<br>Wright Research & Development Center (WRDC) |
| 6c. ADDRESS (City, State, and ZIP Code)<br>21414 - 68th Avenue South<br>Kent, WA 98032 | 7b. ADDRESS (City, State, and ZIP Code)<br>Wright-Patterson AFB, OH 45433-6563 |
| 8a. NAME OF FUNDING / SPONSORING ORGANIZATION<br>Department of the Air Force<br>8b. OFFICE SYMBOL (If applicable) | 9. PROCUREMENT INSTRUMENT IDENTIFICATION NUMBER<br>F33615-89-C-2932 |
| 8c. ADDRESS (City, State, and ZIP Code)<br>Air Force Systems Command<br>Aeronautical Systems Division/PMRNC<br>Wright-Patterson AFB, OH 45433-6503 | 10. SOURCE OF FUNDING NUMBERS<br>PROGRAM ELEMENT NO. 65502F<br>PROJECT NO. 3005<br>TASK NO 21<br>WORK UNIT ACCESSION NO 47 |

11. TITLE (Include Security Classification)
DEVELOPMENT OF A MATHEMATICAL CODE TO PREDICT THERMAL DEGRADATION OF FUEL AND DEPOSIT FORMATION IN A FUEL SYSTEM

12. PERSONAL AUTHOR(S)
Menon, Suresh

| 13a. TYPE OF REPORT | 13b. TIME COVERED | 14. DATE OF REPORT (Year, Month, Day) | 15. PAGE COUNT |
|---|---|---|---|
| Final | FROM 8/15/89 TO 4/15/90 | 1990 September | 50 |

16. SUPPLEMENTARY NOTATION

| 17. COSATI CODES | | | 18. SUBJECT TERMS (Continue on reverse if necessary and identify by block number) |
|---|---|---|---|
| FIELD | GROUP | SUB-GROUP | Thermal Instability, Jet Fuels, Fuel Degradation, Chemical Kinetics, Surface Catalysis, Fuel Deposits, Mathematical Model, Numerical Analysis. |
| 21 | 01 | | |
| 04 | 03 | | |

19. ABSTRACT (Continue on reverse if necessary and identify by block number)

It has been observed in both small-scale experiments and full-scale system simulators that jet fuels, when heated, undergo chemical reactions that eventually result in sediment/deposit formation. Thus, the thermal instability of jet fuels has the deleterious effect of causing fuel system malfunctions. This situation is also possible in supersonic aircraft, where an increase in the metal skin temperature due to aerodynamic heating can, in turn, increase the temperature of uninsulated fuel tanks, leading to deposit formation. Although a great deal of experimental data has been obtained, the exact mechanisms of the degradation reaction and the consequent deposit formation process are still largely unknown. This is primarily due to the fact that the degradation process is influenced by many factors, some of which cannot be determined, varied, or controlled in an experiment. Thus, there is a need for a mathematical model that, once validated, can be used to predict the fuel deposition process by combining the effects of the fluid flow
(continued on next page)

| | |
|---|---|
| 20. DISTRIBUTION / AVAILABILITY OF ABSTRACT<br>☒ UNCLASSIFIED/UNLIMITED ☐ SAME AS RPT. ☐ DTIC USERS | 21. ABSTRACT SECURITY CLASSIFICATION<br>UNCLASSIFIED |
| 22a. NAME OF RESPONSIBLE INDIVIDUAL<br>Capt Jeffrey A. Pearce | 22b. TELEPHONE (Include Area Code) (513) 255-4160<br>22c. OFFICE SYMBOL WRDC/POSF |

DD Form 1473, JUN 86 Previous editions are obsolete

SECURITY CLASSIFICATION OF THIS PAGE
UNCLASSIFIED

19. ABSTRACT (Cont.)

and heat transfer processes and the fuel degradation reactions. In Phase I, such a mathematical model was developed and calibrated using available experimental data. The resulting model appears to contain most of the essential elements for predicting the deposition process and the thermal degradation of jet fuels. However, the full potential of this model cannot be ascertained from the present validation study due to lack of adequate experimental data on many aspects of the physical processes involved in jet fuel thermal degradation. More accurate and innovative experiments are needed to isolate and identify the various physical mechanisms so that the capabilities of the model developed in this study can be evaluated under various operating conditions.

## TABLE OF CONTENTS


1. INTRODUCTION 1
2. TECHNICAL OBJECTIVES 3
3. FORMULATION OF THE MODEL 3
   3.1 Heat Transfer in the Heating Rod 5
   3.2 Heat Transfer Across the Fuel Deposit 7
   3.3 Mass, Momentum, and Heat Transfer in the Fluid Phase 8
      3.3.1 Equation of State 11
      3.3.2 Conservation of Mass 11
      3.3.3 Conservation of Momentum 12
      3.3.4 Conservation of Energy 13
      3.3.5 Reduction of the Two-Phase Equations for the Phase I Model 14
   3.4 Species Transport in the Fluid Phase 16
      3.4.1 Species Transport in the Fluid Phase 16
      3.4.2 Reduction of the Model for the Phase I Study 17
   3.5 Formation of Deposit Due to Fuel Degradation Reactions 19
4. THE NUMERICAL CODE 25
   4.1 The Explicit Scheme 25
   4.2 The Implicit Scheme 26
5. RESULTS AND DISCUSSION 28
6. CONCLUSIONS AND RECOMMENDATIONS 39
REFERENCES 43

## LIST OF FIGURES


| | | |
|---|---|---|
| Figure 1. | An Axisymmetric Fuel Flow System with Characteristic JFTOT Dimensions | 4 |
| Figure 2. | Local Deposit Surface Nonuniformities Due to Random Deposition | 22 |
| Figure 3. | Steady-State Temperature Field in the Heating Rod and in the Fuel with a Constant Heat Flux Boundary and Insulated Ends | 30 |
| Figure 4. | Steady-State Temperature Field in the Heating Rod and in the Fuel with a Parabolic Heat Flux Boundary and Insulated Ends | 32 |
| Figure 5. | Time-Dependent Growth of the Deposit at Peak Temperature Location for Various Models | 35 |
| Figure 6. | Axial Variation of the Deposit Thickness on the Rod Surface | 37 |
| Figure 7. | Axial Variation of the Deposit Precursor and the Fuel Temperature | 38 |
| Figure 8. | Time-Dependent Growth of Deposit Thickness at the Peak Temperature Location for $E_w$ = 8 Kcal/mole | 40 |
| Figure 9. | Axial Variation of Deposit Thickness | 40 |

## 1. INTRODUCTION

It has been observed experimentally that jet fuels, when heated, undergo chemical reactions that eventually result in sediment/deposit formation. In an aircraft engine, under normal operating conditions, the temperature in the fuel supply systems, such as the heat exchanger, fuel lines, and injection nozzles, is typically in the range of 100-300°C. At these temperatures, the fuel tends to undergo degradation reactions, resulting in the formation of deposits. This can adversely affect the operation of the aircraft by clogging the fuel lines and injection nozzles. With the increased use of advanced turbines designed to operate at higher temperatures, thermal degradation problems are expected to increase. Also, in supersonic aircraft, a considerable increase in the metal skin temperature is possible due to aerodynamic heating. For example, it has been estimated that for an aircraft cruising at Mach 2.7, the external skin temperature can reach into the range of 450-500°F (230-260°C), and the temperature of an uninsulated fuel tank could rise to 430°F (220°C). Hydrocarbon fuel exposed to such temperature stress can undergo degradation and form deposits (Taylor, 1969a). Our knowledge of the chemical structure of fuel deposits, the mechanisms for deposit formation, and the locations where the deposits collect is currently limited. By understanding the processes involved, suitable modifications to the fuel, handling techniques, or surface material can be made to eliminate or minimize deposit formation. This would result in improvements in the design of fuel systems for future aircraft.

The susceptibility of hydrocarbon fuel to thermal degradation is usually called thermal instability and is influenced by many factors, such as fuel type, temperature, pressure, and the material in contact with the fuel (Marteney, 1988; Marteney and Spadaccini, 1986; Taylor, 1967, 1969b; CRC, 1978, 1979; Dahlin et al., 1981; Daniel, 1983, 1985). The effects of these factors on the formation of deposits have been investigated experimentally under both nonflowing and flowing conditions. In many of these investigations (e.g., Cohen, 1980; Taylor, 1969b, 1970; Taylor and Frankenfeld, 1978), only the overall rate of deposit was measured. The chemical structure of fuel deposits has been determined in some experiments for various types of jet fuels (e.g., Hemlick and Seng, 1984; Nixon and Henderson, 1966). The presence of molecular oxygen in fuel lines appears to play a major role in the chemical degradation of the fuel (e.g., Nixon and Henderson, 1966; Taylor, 1974) and recent experiments indicate that autooxidation reactions are the primary process of deposit formation at temperatures less than 535K (Marteney, 1988; Marteney and Spadaccini, 1986). However, it has also been observed that deoxygenated fuel forms deposits if the temperature is high enough (Taylor and Frankenfeld, 1978). Deposits formed under these conditions differ in composition from those formed in the presence of oxygen. Furthermore, in deoxygenated fuels, the addition of trace compounds, such as nitrogen compounds, decreases the thermal stability (Nixon, 1962). A similar decrease in stability was observed when trace amounts of sulphur compounds, i.e., thiols, sulfides, and disulfides, were added to deoxygenated hydrocarbon fuels (Taylor, 1976; Taylor and Wallace, 1968). This decrease in stability was attributed to a process of free-radical-initiated chain reactions, although details of the reaction mechanism are unknown. Metal surfaces and dissolved metal salts can also decrease thermal stability (e.g., Schenk et al., 1971; Taylor, 1969b; Kendall and Mills, 1986). On the other hand, removal of molecular oxygen from the fuel has shown an increase in stability, resulting in reduced deposit formation (Taylor, 1974). Thus, the process of thermal degradation of both fuels with molecular oxygen and deoxygenated fuels appears to be influenced by many factors, some of which are still unknown.

The formation of deposits under conditions in which the fuel is flowing over heated surfaces has also been extensively studied. Earlier experiments employed the small-scale thermal stability test devices such as the Jet Fuel Thermal Oxidation Tester or JFTOT (CRC, 1978; UTC, 1988). More recently, an extensive test program was conducted by Marteney (1988) and Marteney and Spadaccini

(1986) to determine the thermal stability and heat transfer characteristics of JP-5 and several kerosene-type fuels using small, resistively heated tubes. Data under various operating conditions was obtained with a high degree of repeatability. It was determined that the surface temperature was the key parameter affecting the deposit formation, although additional parameters such as the fuel flow rate and test duration were also identified as important physical parameters. One of the important results of these studies was that the thermal degradation process occurs in two stages, each with its own unique activation energy. The first stage occurs at relatively low temperatures (less than 535K) and appears to be primarily autooxidation-limited, whereas the second stage occurs at higher temperatures (535-615K) and appears to be combination of autooxidation and hydrocarbon pyrolysis. However, in another set of experiments (Chin et al. 1989), with heated flowing fuels over heated metal surfaces, the deposition characteristics were in many significant respects quite different than Marteney's data. Thus, there are still some unanswered questions regarding the exact thermochemical processes involved in the thermal degradation of jet fuels.

Since experimental studies are at present incapable of providing a detailed understanding of the various phenomena occurring during thermal degradation of jet fuels, there is a need to develop an alternative approach that may provide a fundamental improvement in our understanding of the physics of the degradation process. One such alternative approach is the use of computational fluid dynamics (CFD) to develop models that can be systematically used to study the fluid dynamics, heat transfer, and chemical processes that occur during thermal degradation of jet fuels. Since the various parameters can be varied in a CFD approach relatively easily as compared to the experimental approach, CFD models may provide the necessary flexibility to predict the sensitivity of the parameters that govern the deposition process. However, it is clear that to properly use CFD models, they must first be validated by comparing the predictions with experimental data. Therefore, the availability of accurate experimental data is essential for the successful development of CFD models.

Recently, CFD models have been developed by Oh et al. (1989), Roquemore et al. (1989), and Krazinski et al. (1990). Three-dimensional effects were investigated by Oh et al. (1989), who found that a complex spiraling 3D flow exists in the JFTOT. In the study by Krazinski et al. (1990), a thermal deposition model was incorporated into an existing CFD code which solved the Reynolds-averaged equations of mass, momentum, and energy. Steady-state solutions were obtained using an efficient multigrid technique. The thermal deposition process was modeled by three global Arrhenius reactions in which the thermal decomposition of the fuel was assumed to be primarily due to the autooxidation reaction with the dissolved oxygen in the jet fuel. Since various parameters had to be calibrated, the experimental data of Marteney (1988) and Marteney and Spadaccini (1986) was first employed to calibrate the unknown parameters. The model was then tested on other fuel decomposition data. Good agreement was obtained in these studies for both laminar and turbulent fuel flows.

The CFD model described above, however, had some limitations, some of which are currently being addressed (Roquemore, private communication). For example, the steady-state analysis did not address the nonlinear time-dependent behavior of the deposition process. Experiments by Marteney (1988) showed that as the test duration was increased, the deposition rate also increased. Such a nonlinear, time-dependent phenomena must be modeled using a time-accurate model. Furthermore, the model did not account for the formation of solid particles in the flowing fuel and its subsequent transport and impaction on the wall. As the deposit grows on the wall, it will affect the heat transfer between the heated rod and the fuel (Marteney, 1988), a process that was also not modeled in the above-mentioned study. In spite of these limitations, the results obtained so far are quite impressive in demonstrating the capability of the CFD approach to model and predict the fuel decomposition and deposit formation process.

In the Phase I study described here, a mathematical model was developed that takes into account the time-dependent interactions among the heat transfer in the heating element, the heat transfer across the thin layer of deposit, the heat loss to the flowing fluid and the chemical kinetics of the fuel degradation reactions. The complex coupling among the unit processes is modeled by a system of differential equations. In many respects, the model developed here is similar to the CFD model developed by Roquemore et al. (1989) and Krazinski et al. (1989). There are some differences, however, which will become apparent in the subsequent sections. For demonstration purposes, a simple fuel flow system is chosen which approximately models a small-scale test device (i.e., JFTOT) that has been used extensively in many experimental studies. The results of this study are documented in this report.

## 2. TECHNICAL OBJECTIVES

The objectives of the Phase I research were as follows:

1. To construct a mathematical model of fuel deposition in a simple flowing system by using existing knowledge on each unit process.
2. To demonstrate the mathematical model by applying it to a simple fuel system with known experimental results.
3. To compare the results with experimental measurements.

As described in this report, all these objectives have been successfully achieved.

## 3. FORMULATION OF THE MODEL

In this section, we describe in some detail the formulation of the model. The formulation was carried out in a general sense so that eventual application to realistic fuel systems could be carried out in the next phase. However, since there are various aspects of the coupling and the chemical kinetics that are still poorly understood, some simplifications to the full model were made before carrying out the computations. These simplifications will be discussed later.

Due to the limited resources available for the Phase I research, we investigated a fuel flow system with a simple model. The fuel system modeled is the JFTOT test device configuration used in the experiments. It is well-known that the flow field in the JFTOT is three-dimensional (CRC, 1978, 1979; UTC, 1988; Oh et al., 1989); however, for this phase of study we restrict ourselves to axisymmetric geometry. Extension to three-dimensional flow can be accomplished in the next phase. The flow configuration considered here is shown in Figure 1. It consists of a circular pipe of length $l$ and internal diameter of $2r_3$, with a heating rod of diameter $2r_1$ at the center. The rod is heated by an electrical element at its center so that the heating process can be simulated by a prescribed heat flux condition at the centerline. This is similar to the experimental condition of Marteney and was also used in the CFD model developed by Roquemore et al. (1989) and Krazinski et al. (1989). However, the CFD code was written using a general format so that various types of boundary conditions can be implemented easily without any major modifications.

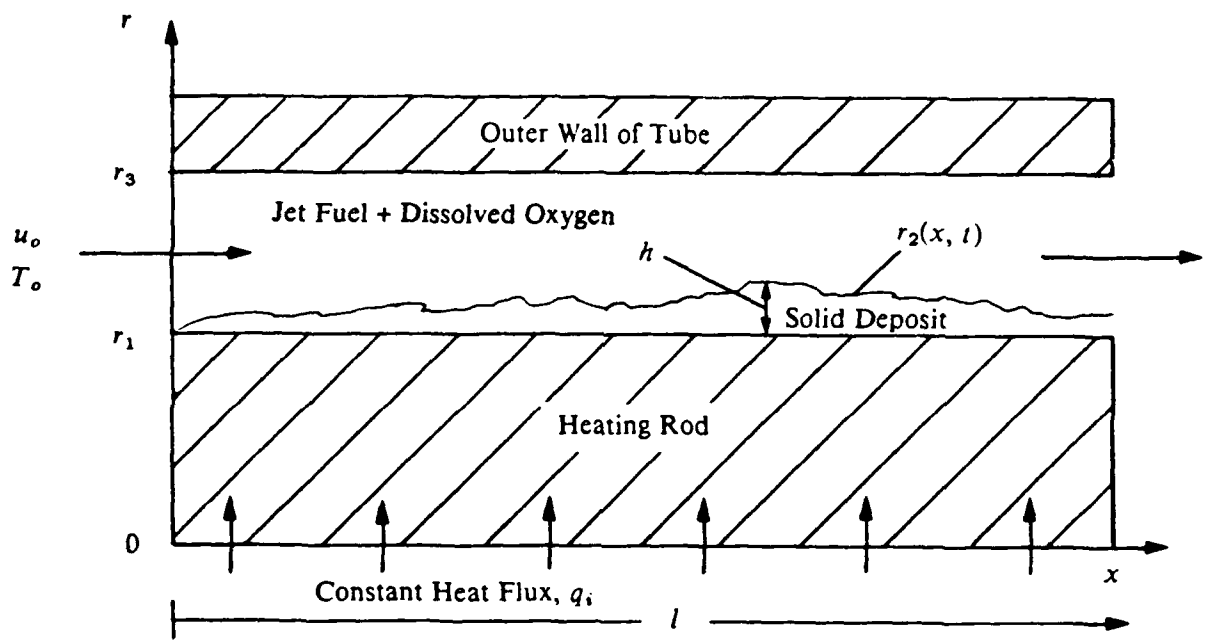


**Figure 1. An Axisymmetric Fuel Flow System with Characteristic JFTOT Dimensions**

There are five main unit processes that must be modeled and coupled together to simulate the problem of deposit formation due to thermal degradation of the flowing fuel:

1. Heat transfer in the heating rod.
2. Heat transfer across the fuel deposit.
3. Mass, momentum, and heat transfer in the fluid phase.
4. Solid and fuel-soluble deposit production and transport in the fluid phase.
5. Formation of the solid deposit on the heated wall due to fuel degradation reactions.

These five unit processes are described separately in the following subsections. Note that the third and fourth unit processes are coupled phenomena in the fluid phase that must be modeled together.

Nondimensionalization

To implement the model into a computational code, it is preferable that the governing equations be nondimensional. Therefore, all the equations were nondimensionalized by choosing reference quantities. We chose a reference length $L$ which for the present study was the radius of the heating rod ($r_1$). A reference velocity $u_r$ was chosen for the flowing fuel and taken to be the mean free stream velocity of the fuel at the inlet. The reference time scale is thus $t_r = L/u_r$. The reference temperature $T_r$ was chosen to be the temperature of the fuel at the inlet (typically room temperature). All transport properties, such the kinematic viscosity of the fuel $\mu_f$ and the thermal conductivities of the rod ($\kappa_s$), the deposit ($\kappa_d$), and the fuel ($\kappa_f$), are nondimensionalized by their respective values at the reference temperature ($T_r$).

In the following formulation, the equations are presented primarily in the dimensional form, although in most cases the effect of nondimensionalization is also described. All dimensional quantities have units consistent with the metric system.

### 3.1 Heat Transfer in the Heating Rod

The first unit process that needs to be modeled is the heat transfer process in the heating rod. The model for the heating rod consists of the heat source at a given location, the axial and radial heat transfer in the rod, and the heat loss to the deposit layer due to conduction. The equation governing the temperature distribution in the rod can be written as

$$\rho_s C_{p_s} \frac{\partial T_1}{\partial t} = \nabla \cdot (\kappa_s \nabla T_1) \tag{1}$$

where $T_1$ is the temperature in the rod and $\kappa_s$, $\rho_s$, and $C_{p_s}$ are the thermal conductivity coefficient, the density of the rod material, and the specific heat of the rod material, respectively. In the JFTOT, the rod is made of stainless steel. For the present study, the density ($\rho_f$) and the specific heat ($C_s$) are assumed to be constants in the temperature range studied, while the thermal conductivity of the stainless steel rod is a weak function of the temperature. Thus, $\kappa_s$ is prescribed by a second-order polynomial in temperature (i.e., $\kappa_s = a + bT + cT^2$), where the coefficients are determined by fitting the polynomial to the data in the temperature range of 100-500°C.

In Equation (1), $\nabla$ is, in general, the three-dimensional differential operator. For the present study, we reduce it to the axisymmetric differential operator so that after nondimensionalizing, the final equation for transport of heat in the rod can be written as

$$\bar{\rho}_e \bar{C}_{p_e} \frac{\partial \bar{T}}{\partial \bar{t}} = \sigma_e \left[ \frac{\partial}{\partial \bar{x}} \left( \bar{\kappa}_e \frac{\partial \bar{T}}{\partial \bar{x}} \right) + \frac{1}{\bar{r}} \frac{\partial}{\partial \bar{r}} \left( \bar{r} \bar{\kappa}_e \frac{\partial \bar{T}}{\partial \bar{r}} \right) \right] \tag{2}$$

where the bar denotes the nondimensional quantities and, for simplicity, the subscript 1 in Equation (1) has been neglected. Also, $\sigma_e$ is a constant that appears due to the nondimensionalization and is defined as

$$\sigma_e = \frac{\kappa_{e_r}}{\rho_{e_r} C_{p_{e_r}} u_r L} = \frac{\rho_{f_r}}{\rho_{e_r}} \frac{C_{p_{f_r}}}{C_{p_{e_r}}} \frac{\kappa_{e_r}}{\kappa_{f_r}} \left[ \frac{1}{\mathrm{Re}_L Pr_r} \right] \tag{3}$$

where the rod transport properties have been rescaled using the reference values for the fuel. Here, $\mathrm{Re}_L = \rho_{f_r} u_r L / \mu_{f_r}$ is the Reynolds number of the fuel flow based on the reference length $L$ and fuel properties at the reference temperature, and $Pr_r = \mu_{f_r} C_{p_{f_r}} / \kappa_{f_r}$ is the Prandtl number of the fuel at the reference temperature. The physical domain in which this equation is valid is defined by $0 < x < l$ in the axial direction, where $l$ is the length of the rod, and by $0 < r < r_1$ in the radial direction, so that when nondimensionalized, the axial domain is $0 < \bar{x} < l/r_1$ and the radial domain is $0 < \bar{r} < 1$.

Equation (2) is solved subject to proper boundary conditions. The formulation allows us to implement any type of boundary conditions at the boundaries. Therefore, in general, the dimensional boundary conditions for the heating rod are

$$\kappa_e \frac{\partial T_1}{\partial x} = q_0 \qquad \text{at } x = 0 \tag{4}$$

$$\kappa_e \frac{\partial T_1}{\partial x} = q_l \qquad \text{at } x = l \tag{5}$$

$$\frac{\partial T_1}{\partial r} = q_i \qquad \text{at } r = 0 \tag{6}$$

$$\kappa_e \frac{\partial T_1}{\partial r} = \kappa_d \frac{\partial T_2}{\partial r} \qquad \text{at } r = r_1 \tag{7}$$

Here, the subscript 1 denotes the variables in the heating rod, and the subscript 2 denotes those in the deposit layer. The boundary conditions at $x = 0$ and $x = l$ allows the possibility of heat loss (if $q_0 < 0$ and $q_l < 0$) or heat addition (if $q_0 > 0$ and $q_l > 0$) or insulated wall (if $q_0 = q_l = 0$). There is also an option to use constant temperature end conditions [i.e., $T(x = 0) = T_r$ and $T(x = l) = T_r$]. If the rod is heated by a heating element as is modeled in the present JFTOT configuration, then at $r = 0$, the heat flux is prescribed by $q_i$. Finally, the boundary condition given by Equation (7) determines the heat loss from the heating rod to the deposit layer.

### 3.2 Heat Transfer Across the Fuel Deposit

The second unit process is the heat transfer across the deposit layer. The deposit is defined by the axial domain $0 < x < l$ and the radial domain of $r_1 < r < r_2$. Note that the deposit thickness will grow in the axial direction and in time and thus, $r_2 = r_2(x, t)$. Since the deposit layer is usually very thin, the heat transfer in the deposit layer can be modeled as a steady-state process, i.e., the equation governing the heat conduction through the layer is then

$$\nabla \cdot (\kappa_d \nabla T_2) = 0 \tag{8}$$

Furthermore, since the layer is very thin, the axial variation of temperature in the deposit can be neglected when compared to its radial variation. Thus, Equation (8) reduces to a one-dimensional form:

$$\frac{\partial}{\partial r}\left[r \kappa_d \frac{\partial T_2}{\partial r}\right] = 0 \tag{9}$$

This equation can be directly integrated to obtain

$$\int_{T_1^+}^{T_2^-} \kappa_d dT = \int_{r_1}^{r_2} \frac{C_d}{r} dr \tag{10}$$

where $C_d$ is the as yet unknown constant of integration, $T_1^+$ is the temperature of the deposit just above the heated rod at $r = r_1$, and $T_2^-$ is the temperature of the deposit just below the fuel at $r = r_2$. The boundary conditions for this equation are

$$\kappa_d \frac{\partial T_2}{\partial r} = \kappa_f \frac{\partial T_3}{\partial r} \qquad \text{at } r = r_2 \tag{11}$$

and the condition given by Equation (7) at $r = r_1$. In Equation (11), the subscript 3 denotes the fluid phase. When the heat flux conditions are matched at $r = r_1$ and $r = r_2$, then $T_1^+ = T_1(r = r_1) = T_2(r = r_1)$, and $T_2^- = T_2(r = r_2) = T_3(r = r_2)$.

To solve Equation (10), the thermal conductivities of the deposit material, $\kappa_d$, and of the fuel, $\kappa_f$, are required. In the present study, we use JP-5 as the jet fuel and the properties of JP-5 as a function of temperature were explicitly employed from the curve fits provided to us by the sponsor. Thus, the thermal conductivity of JP-5 in $(J/mK - s)$ is

$$\kappa_f = A + BT + CT^2 \tag{12}$$

where $A = 0.2503$, $B = -5.6363 \times 10^{-4}$, and $C = 4.7482 \times 10^{-7}$. We further assumed that the thermal conductivity of the deposit, $(\kappa_d)$, is also related to temperature by the same functional relation as in Equation (12), but since the deposit thermal conductivity is probably much lower than that of the fluid, we assume $\kappa_d = A_d \kappa_f$ ,where $A_d < 1$ is a constant input parameter. Using the relation between $\kappa_d$ and $\kappa_f$ in Equation (10), a cubic equation is obtained which can be written in the nondimensional form as

$$\frac{A^*}{3}(T_2^3 - T_1^3) + \frac{B^*}{2}(T_2^2 - T_1^2) + C^*(T_2 - T_1) = C_d \ln(1 + \bar{h}) \tag{13}$$

where $A^* = AT_r^2/\kappa_{d_r}$, $B^* = BT_r/\kappa_{d_r}$, and $C^* = C/\kappa_{d_r}$ are constants. Here $\bar{h} = (r_2 - r_1)/r_1$ is the nondimensional thickness of the deposit, which is a variable in this problem. Since the deposit growth is both time- and space-dependent in the present formulation, the thickness $\bar{h} = \bar{h}(\bar{x}, t)$ and $r_2 = r_2(x, t)$. In Equation (13) we have neglected the superscripts + and − for simplicity and the nondimensional temperatures $T_1$ and $T_2$ are the temperatures at $\bar{r} = 1$ and $\bar{r} = 1 + \bar{h}$, respectively. At this stage, there are three unknowns in Equation (13), i.e., $T_1$, $T_2$, and $C_d$. To determine these unknowns, we combine Equation (13) with the boundary conditions, Equation (7) at $\bar{r} = 1$ and Equation (11) at $\bar{r} = 1 + \bar{h}$. The nondimensional form of Equation (7) can be written using standard one-sided difference as

$$T_1(\bar{r} = 1) = T_1(\bar{r} = 1 - \Delta r_1) + \alpha_1 C_d \tag{14}$$

Similarly, Equation (11) can be written as

$$T_2(\bar{r} = 1 + \bar{h}) = T_2(\bar{r} = 1 + \bar{h} + \Delta r_2) - \alpha_2 C_d \tag{15}$$

where the differential form of Equation (10) has been used and

$$\alpha_1 = \left[\frac{\kappa_{d_r}}{\kappa_{e_r}}\right]\left[\frac{\Delta r_1}{\overline{\kappa_e}}\right]$$

and

$$\alpha_2 = \left[\frac{\kappa_{d_r}}{\kappa_{f_r}}\right]\left[\frac{\Delta r_2}{(1 + \bar{h})\overline{\kappa_f}}\right]$$

Here, $\overline{\kappa_e}$ and $\overline{\kappa_f}$ are the nondimensional thermal conductivities of the rod and the fluid, respectively. Also, $\Delta r_1$ and $\Delta r_2$ are the nondimensional grid spacing in the rod and in the fluid, respectively. Note that in Equations (14) and (15), only first-order accurate differencing is employed. However, a second-order accurate one-sided difference can be used and in fact was employed in the code. Combining Equations (13) through (15), we obtain a cubic equation for $C_d$. The real root of this equation is the solution for $C_d$. Once $C_d$ is known, Equations (14) and (15) can be used to determine the temperatures at $\bar{r} = 1$ and $\bar{r} = 1 + \bar{h}$. Note that when there is no deposit ($\bar{h} = 0$), then $T_1 = T_2$, i.e, the fuel and the rod are at the same temperature at their interface. However, when $\bar{h} \neq 0$, the cubic equation must be solved at each time step and at each axial location to match the gradients and thus obtain the temperature of the rod at $\bar{r} = 1$ and the temperature of the fuel at $\bar{r} = 1 + \bar{h}$.

An advantage of this formulation is that it allows us to adjust the temperatures of the rod and the fuel depending upon the heat transfer characteristics of the deposit. Thus, when $A_d < 1$ is given, the deposit will inhibit the heat transfer from the rod to the fuel and the temperature of the rod at $\bar{r} = 1$ will increase while the temperature of the fuel at $\bar{r} = 1 + \bar{h}$ will decrease. This is exactly the physical phenomena observed in the experiments by Marteney (1988).

### 3.3 Mass, Momentum, and Heat Transfer in the Fluid Phase

The fuel deposit will form due to the degradation reactions that occur when the fuel is heated. Since the heat source is a metal rod, the deposit will form near the surface of the rod due to the surface catalytic mechanism. This catalytic mechanism is very complex and depends on various factors, including the properties of the fuel and the surface material (e.g., Taylor, 1969b). We shall discuss this mechanism in a later section. In addition to this mechanism of deposit formation, if the fuel is

thermally unstable in the fluid layer near the high-temperature surface, then the fuel can undergo degradation reactions, resulting in deposit formation in the bulk fuel itself. The deposit that forms in the liquid fuel could have two very different characteristics. It is reasonable to assume that under some conditions, the deposit that forms due to chemical reactions in the bulk fuel will be liquid product, i.e., the deposit can be considered a liquid precursor which may eventually undergo a phase change and condense into solid form. In addition to this liquid deposit precursor, solid particles similar to the deposit on the heated wall may also form in the bulk fuel. Both the deposit precursor and the solid particles can migrate to the wall due to diffusion processes and become a part of the deposit on the surface. A reverse migration process is also possible due to the fluid motion in which the solid deposit on the wall is entrained into the flow due to abrasion and flaking. For example, in wing fuel tanks containing puddles of residual liquid hydrocarbon and hydrocarbon vapor, the fuel deposits have a tendency to flake off, contaminate the fuel, and cause the fuel system to malfunction (e.g., Taylor, 1969a).

Thus, to model the fluid phase transport, we need to consider the general mass, momentum, and heat transfer in a multicomponent chemical fluid mixture in which some solid particles may also be present. The model equations must be a generalized version of a two-phase mixture of fluid and solid particles. In this section, we will develop a general model for this problem which allows for the phase transition of the liquid deposit precursor into solid particles. However, since this is a complex model, we will not implement it in this phase. After deriving the general model, we will reduce it to a form which is simple enough to be considered in the Phase I study described here.

Before deriving the general governing equations, some basic assumptions are required to maintain the tractability of the equations. Although some of these assumptions are quite reasonable, some will have to be reexamined in a later study when additional experimental data is available.

The primary assumptions used to derive these two-phase flow equations are:

1. The "bulk fuel" is a mixture of three species: the fuel, the dissolved oxygen, and the liquid deposit precursor.
2. Solid deposits may be present in the "bulk fuel" due to phase change of the liquid precursor, but are assumed to occupy only a small fraction of the total volume of the bulk fuel.
3. The solid deposit in the "bulk fuel" is mixed well with the fuel so that the solid particles can be considered a pseudofluid, thereby allowing the derivation of the solid particle transport equations from the continuum theory.
4. All solid particles in the "bulk fuel" are of the same size and can be approximated by a spherical shape of radius $r_p$. Thus, the drag coefficient of all the particles is the same in the fuel.

Before deriving the conservation equations, some fundamental definitions must be given. We consider a two-phase mixture of "bulk fuel" and solid particles. It must be noted, however, that the "bulk fuel" itself is a mixture of three species (fuel, dissolved oxygen, and liquid deposit precursor). Differentiation between the three species will be made only when deriving the energy transport and the bulk fuel species transport equations.

We define a solid particle in the bulk fuel with a mass $m_p$, a radius $r_p$, and a specific heat $C_s$, all of which are assumed constant. An element of the mixture of bulk fuel and solid particles has a total mass $M = M_f + M_p$, and a total volume $V = V_f + V_p$, where the subscripts $f$ and $p$ denote the bulk

fuel and solid particles, respectively. If the total number of solid particles in the bulk fuel is given by its number density per unit volume, $n_p$, then the total volume occupied by all the particles, $V_p$, is

$$V_p = n_p V \frac{4}{3} \pi r_p^3 = n_p V v_p \tag{16}$$

where $v_p$ is the volume of a single particle. The total mass occupied by all the solid particles is given by

$$M_p = m_p n_p V \tag{17}$$

Thus, the species density of the solid particles is

$$\rho_{sp} = \frac{M_p}{V_p} = \frac{m_p}{v_p} \tag{18}$$

For a given fuel, the species density of the solid particle may be assumed a known constant.

For a two-phase mixture, we need to know the partial densities of the pseudofluid of the solid particles and the fuel. We define the partial density of the particles as

$$\overline{\rho_p} = \frac{M_p}{V} = m_p n_p = \rho_{sp} v_p n_p \tag{19}$$

and define the volume fraction of the solid particles in the two-phase mixture, $\lambda$, as

$$\lambda = \frac{V_p}{V} = n_p v_p = \frac{\overline{\rho_p}}{\rho_{sp}} \tag{20}$$

In this formulation, $\lambda$ is a principle dependent variable representing the pseudofluid of solid particles in the bulk fuel. When $\lambda \ll 1$ the equations can be further reduced to the form representing dilute mixtures (Pai, 1977). However, in the present formulation, $\lambda < 1$ may be possible. The theory described here is valid for finite values of $\lambda$.

Similar to the above definitions, we define the species density of the bulk fuel as

$$\rho_f = \frac{M_f}{V_f} \tag{21}$$

and its partial density as

$$\overline{\rho_f} = \frac{M_f}{V} = \frac{M_f}{V_f} \frac{V_f}{V} = (1 - \lambda)\rho_f \tag{22}$$

With these basic definitions we can derive the conservation equations for a mixture of bulk fuel and pseudofluid of solid particles.

### 3.3.1 Equation of State

Each species will have its own equation of state. For the solid particles in a given fuel, we may assume

$$\rho_{sp} = constant \tag{23}$$

For the bulk fuel, the equation of state may be prescribed as

$$\rho_f = \rho_f(T_f) \tag{24}$$

where $T_f$ is the temperature of the bulk fuel. This relationship, Equation (24), may be assumed given for a given fuel. For example, from the curve fit for JP-5, the fuel density in $(kg/m^3)$ is

$$\rho_f = 810.37 + 0.4004T_f - 1.3582\times10^{-3}T_f^2$$

### 3.3.2 Conservation of Mass

The conservation of mass for both phases of the mixture can be written separately as follows.

*Solid Phase*

$$\frac{\partial \rho_{sp}\lambda}{\partial t} + \frac{\partial \rho_{sp}\lambda u_{p_i}}{\partial x_i} = \sigma_p \tag{25}$$

Here, the relation $\overline{\rho_p} = \rho_{sp}\lambda$ has been used, and since $\rho_{sp}$ is assumed a constant [Equation (23)], Equation (25) is an equation for $\lambda$. Also, $u_{p_i}$ are the velocity components in the three spatial directions of the pseudofluid of solid particles in the two-phase mixture. The source term $\sigma_p$ indicates that there may be a phase transition of the precursor fuel-soluble product into solid particles. If $\sigma_p = > 0$, then the precursor fuel-soluble deposit will convert to solid particles. At present, we will not address the functional relationship of $\sigma_p$.

*Bulk Fuel Phase*

$$\frac{\partial \rho_f(1-\lambda)}{\partial t} + \frac{\partial \rho_f(1-\lambda)u_{f_i}}{\partial x_i} = -\sigma_p \tag{26}$$

Here, $u_{f_i}$ are the three velocity components of the bulk fuel. The mass sink in the bulk fuel continuity equation implies that during phase transition of the liquid precursor into solid deposit there will be equivalent loss in the bulk fuel mass.

Note that if we add Equations (25) and (26) and define a mixture density $\rho_M$ as

$$\rho_M = \overline{\rho_p} + \overline{\rho_f} = \lambda\rho_{sp} + (1-\lambda)\rho_f \tag{27}$$

we get the conservation of mass of the mixture as

$$\frac{\partial \rho_M}{\partial t} + \frac{\partial \rho_M u_{M_i}}{\partial x_i} = 0 \tag{28}$$

where the mixture velocity $u_{M_i}$ is given as

$$u_{M_i} = \left[\overline{\rho_p}u_{p_i} + \overline{\rho_f}u_{f_i}\right]/\rho_M \tag{29}$$

### 3.3.3 Conservation of Momentum

The conservation of momentum for both phases are also written separately.

*Solid Phase*

$$\frac{\partial \lambda \rho_{sp} u_{p_i}}{\partial t} + \frac{\partial}{\partial x_j}\left[\lambda \rho_{sp} u_{p_i} u_{p_j} + p_p \delta_{ij} - \tau_{ij}{}^p\right] = F_{p_i} + F_{p\sigma_i} \tag{30}$$

where $p_p = \lambda p$ is the partial pressure of the solid phase and $p$ is the pressure in the mixture. Also, $\tau_{ij}{}^p$ is the viscous stress tensor of the pseudofluid, which by definition of a pseudofluid may be modeled in the classical form as a function of the viscosity of the pseudofluid ($\mu_p$) and the gradients in the pseudofluid velocity ($u_{p_i}$). The forces $F_{p_i}$ and $F_{p\sigma_i}$ are, respectively, the i-th component of the solid-liquid interaction force and the force resulting from the mass source $\sigma_p$.

*Bulk Fuel Phase*

$$\frac{\partial (1-\lambda)\rho_f u_{f_i}}{\partial t} + \frac{\partial}{\partial x_j}\left[(1-\lambda)\rho_f u_{f_i} u_{f_j} + p_f \delta_{ij} - \tau_{ij}{}^f\right] = F_{f_i} + F_f \sigma_i \tag{31}$$

Here, $p_f = (1-\lambda)p$ is the partial pressure of the bulk fuel and $\tau_{ij}{}^f$ is the viscous stress tensor for the bulk fuel, which is a function of the fuel kinematic viscosity $\mu_f$ and the velocity gradients. $F_{f_i}$ is the interaction force between the fluid and the pseudofluid of particles, and $F_{f\sigma_i}$ is the force due to the mass source $\sigma_p$.

As a first approximation, the viscous stress tensor for both the pseudofluid of solid particles and the bulk fuel can be expressed from continuum theory as

$$\tau_{ij}{}^n = \mu_{n_1}\left[\frac{\partial u_{n_i}}{\partial x_j} + \frac{\partial u_{n_j}}{\partial x_i}\right] + \mu_{n_2}\left[\frac{\partial u_{n_k}}{\partial x_k}\right]\delta_{ij}$$

where $n$ stands for either the fluid ($f$) or the solid phase ($p$), $\mu_{n_1}$ is the viscosity of the nth species, and $\mu_{n_2} = -2/3\mu_{n_1}$ is the bulk viscosity.

By the third law, we have

$$\vec{F_f} = -\vec{F_p} \tag{32}$$

and

$$\vec{F_{p\sigma}} = -\vec{F_{f\sigma}} \tag{33}$$

The interaction force ($\vec{F_f}$ or $\vec{F_p}$) is usually a very complex function of the drag coefficient ($C_D$), the radius of the particles, the number density ($n_p$), and the difference in the velocities ($u_{p_i} - u_{f_i}$). The functional form of this force will have to be prescribed to close the equations. As a first approximation, we may take for very slow flow (i.e., for low Reynolds number flows), the Stokes flow approximation for the interaction force (Pai, 1977):

$$F_{p_i} = 6\pi r_p \mu_f n_p \left[\vec{u_f} - \vec{u_p}\right] \tag{34}$$

where we have assumed that the particle-particle interaction can be neglected and $\lambda < 0.1$ applies, so that the Stokes form for drag is applicable. When $0.1 < \lambda < 1$ occurs, then some modification to the Stokes law will have to be made. There are some representative expressions for the interaction force in the two-phase flow literature which could be used here (Pai, 1977).

The momentum source, $\vec{F}_{f_\sigma}$ (or $\vec{F}_{p_\sigma}$), is a function of the mass source $\sigma_p$ when there is phase change. As a first approximation, we may consider $\vec{F}_{p_\sigma} \approx \sigma_p \vec{u}_p$.

3.3.4 Conservation of Energy

Again, the conservation of energy of both the pseudofluid of solid particles and the bulk fuel can be written separately.

*Solid Phase*

We first define the total energy of the pseudofluid of the solid particle $E_p$ as the sum of its internal energy $e_p$ and its kinetic energy as

$$E_p = e_p + \frac{1}{2} u_{p_i}^2 \tag{35}$$

so that the energy conservation equation can be written as

$$\frac{\partial}{\partial t}\left[\lambda \rho_{sp} E_p\right] + \frac{\partial}{\partial x_i}\left[\lambda \rho_{sp} u_{p_i} E_p - (u_{p_j} \tau_{ji}^p - q_{p_i}) + \lambda u_{p_i} p\right] = \kappa_T (T_f - T_p) + \epsilon_p \tag{36}$$

where $e_p = C_s T_p$ is the internal energy of the pseudofluid, $\epsilon_p$ is the energy source due to chemical reactions or heat addition, and $\kappa_T$ is an interaction coefficient which is typically a function of $r_p$, $n_p$, and $\kappa_p$. Consistent with the Stokes law approximation used in the interaction force for the momentum equation, the relation $\kappa_T = 4\pi r_p \kappa_p n_p$ can be used (Pai, 1977). Here, $\kappa_p$ is the thermal conductivity of the solid particles.

In Equation (36), $q_{p_i}$ is the heat conduction term which is given as

$$q_{p_i} = -\kappa_p \frac{\partial T_p}{\partial x_i} \tag{37}$$

*Bulk Fuel Phase*

Similar to the pseudofluid energy equation, an energy equation for the bulk fuel can be written as

$$\frac{\partial}{\partial t}\left[(1-\lambda)\rho_f E_f\right] + \frac{\partial}{\partial x_i}\left[(1-\lambda)\rho_f u_{f_i} E_p - (u_{f_j} \tau_{ji}^f - q_{f_i}) + (1-\lambda) u_{f_i} p\right] = \kappa_T (T_p - T_f) + \epsilon_f \tag{38}$$

Note that the interaction term appearing on the right-hand-side of this equation is the negative of the interaction term in the pseudofluid energy conservation equation. The meaning of all terms in this equation are similar to those in the pseudofluid equation.

The definition of the total energy for the bulk fuel, $E_f$, is similar to that for the pseudofluid (i.e., $E_f = e_f + u_{f_i}^2/2$). However, since the bulk fuel is considered a mixture of three species, some further modification to the internal energy of the bulk fuel, $e_f$, must be made. Thus, when there are three species in the bulk fuel, the basic definition of internal energy

$$\rho_f e_f = \rho_f C_{v_f} T_f \tag{39}$$

must be reinterpreted as

$$\rho_f e_f = \sum_{k=1}^{3} \rho_{f_k} e_{f_k} \tag{40}$$

where $k = 1,3$ represents the three species in the bulk fuel and $e_{f_k}$ are the k-th species internal energy. If we define a mass fraction $Y_k = \rho_{f_k}/\rho_f$, then the internal energy of the mixture of three species becomes

$$e_f = \sum_{k=1}^{3} Y_k C_{v_k} T_f \tag{41}$$

where $C_{v_k}$ is the specific heat of the k-th species.

Equations (23-26), (30), (31), (36), and (38) are the general conservation equations; provided that all the other auxiliary relations are defined, these equations can be solved for the dependent variables $\lambda$, $u_{p_i}$, $u_{f_i}$, $\rho_f$, $T_p$, and $T_f$. If the bulk fuel is assumed to be a mixture of three species, then additional equations for the species conservation in the bulk fuel, $Y_k$, must be solved. This is described in the next section.

Note that in the present formulation, we have assumed that the bulk fuel is laminar. However, in high Reynolds number flows, the fluid may be turbulent. In these cases, the laminar transport properties (i.e., $\mu_f$, $k_f$, etc., in these equations) can be replaced by the sum of the laminar and turbulent transport properties. The turbulent properties can then be modeled by a conventional turbulence model such as the $k-\epsilon$ model. This would increase the number of equations to be solved in the bulk fuel and increase the computational overhead. For fuel flows in which turbulent effects cannot be ignored, however, a turbulence model must be included. This could be considered in the next phase.

### 3.3.5 Reduction of the Two-Phase Equations for the Phase I Model

The equations derived above are very complex and the full treatment of the two-phase problem is beyond the scope of the Phase I study. Therefore, we consider a much simpler model in the first phase. The first basic assumption is to assume that there are no solid particles in the bulk fuel, i.e., $\lambda = 0$. This immediately reduces the system of equations by half. The next major simplification is to assume that the bulk fuel is being transported by a prescribed axial velocity, $u_f$, so that for an axisymmetric configuration, $u_{f_i} = (u_f, 0)$. Further, we assume $u_f = u_f(r)$. Using these assumptions and further relating the bulk fuel density to the bulk fuel temperature, i.e., $\rho_f = \rho_f(T_f)$ by a prescribed relation (from the curve fits for JP-5), we can decouple the energy transport equation from the mass and momentum equations. Therefore, the only equation that needs to be solved in the bulk fuel phase is the energy equation for the bulk fuel. Using these assumptions and assuming there are no sources in the fluid, the conservation equation for the bulk fuel energy can be reduced to

$$\frac{\partial \rho_f E_f}{\partial t} + \frac{\partial}{\partial x_i}\left[\rho_f E_f + p\right] u_{f_i} = -\frac{\partial q_{f_i}}{\partial x_i} + \frac{\partial}{\partial x_i}\left(u_{f_j}\tau_{ji}\right) \tag{42}$$

If we further define the total enthalpy as $H_f = E_f + p/\rho_f$, Equation (43) can be rewritten as

$$\frac{\partial}{\partial t}(\rho_f H_f - p) + \frac{\partial}{\partial x_i}(\rho_f H_f u_{f_i}) = -\frac{\partial q_{f_i}}{\partial x_i} + \frac{\partial}{\partial x_i}(u_{f_j}\tau_{ji}) \tag{43}$$

Since we are prescribing the fluid velocity at present as $u_{f_i} = (u(r),0)$, and assuming that the pressure is constant in the JFTOT, we can further reduce this equation for axisymmetric flows to

$$\rho_f\left[\frac{\partial h}{\partial t} + u\frac{\partial h_f}{\partial x}\right] = \frac{\partial}{\partial x}\left[\kappa_f\frac{\partial T_f}{\partial x}\right] + \frac{1}{r}\frac{\partial}{\partial r}\left[r\kappa_f\frac{\partial T_f}{\partial r}\right] + \frac{1}{r}\frac{\partial}{\partial r}\left[r\mu_f u_f\frac{\partial u_f}{\partial r}\right] \tag{44}$$

where $\rho_f(T_f)$ is given and the static enthalpy of the fuel is related to the total enthalpy by the relation $H_f = h_f + u_f^2/2$. The static enthalpy is related to the temperature of the fuel by the relation, $h_f = C_{p_f}T_f$. If the bulk fuel is considered to be a mixture of three species, however, this definition is modified to

$$h_f = \sum_{k=1}^{3} Y_k C_{p_k} T_f \tag{45}$$

where $C_{p_k}$ is k-th species specific heat at constant pressure.

Using Equation (45) in Equation (43), we finally obtain an equation for the temperature of the fuel $T_f$. The only unknown in this equation is the species mass fraction, $Y_k$, which will have to be determined. This is described in more detail in the next section.

Equation (43) is solved subject to proper boundary conditions. These are:

$$\kappa_f\frac{\partial T_f}{\partial r} = \kappa_d\frac{\partial T_d}{\partial r} \qquad \text{at } r = r_2 \tag{46}$$

$$\frac{\partial T_f}{\partial r} = 0 \qquad \text{at } r = r_3 \tag{47}$$

$$T_f = T_o \qquad \text{at } x = 0 \tag{48}$$

$$\frac{\partial T_f}{\partial x} = 0 \qquad \text{at } x = l \tag{49}$$

where $T_f$ and $T_d$ are the temperatures of the bulk fuel and of the solid deposit, respectively.

### 3.4 Species Transport in the Fluid Phase

#### 3.4.1 Conservation of Species

Since the bulk fuel is assumed to be a mixture of three species, species transport for each species must be modeled. We consider the situation were the formation of the liquid deposit precursor is due to the reaction between the fuel and the dissolved oxygen, as shown by

$$Fuel + Oxygen \rightarrow Deposit\ Precursor \tag{50}$$

at a rate that is currently modeled by a simple one-step Arrhenius rate. More experimental data is needed to validate this assumption. Therefore, the general conservation equation for the k-th species can be written in terms of the concentration of the k-th species as

$$\frac{\partial [C_k]}{\partial t} + \frac{\partial}{\partial x_i}\left[u_{f_i} + u_{f_{k_i}}[C_k]\right] = P_{C_k} - L_{C_k} \tag{51}$$

where $[C_k]$ is the concentration of the k-th species in the bulk fuel and $u_{f_{k_i}}$ is the diffusion flux velocity of the k-th species in the i-th direction. The diffusion velocity is usually given by Fick's law. The last two terms are, respectively, the production and destruction terms for the k-th species. For the present discussion, we identify $k = 1$ with the fuel (subscript *fu*), $k = 2$ with the dissolved oxygen (subscript *O*), and $k = 3$ with the deposit precursor (subscript *pre*). The use of a simple Arrhenius rate for the production and destruction terms is a simplification of the complex chemical kinetics occurring in the conversion of the fluid to the deposit precursor. As a first approximation, the production of the deposit precursor in the bulk fuel can be modeled as

$$P_{Y_{pre}} = A_{pre}\exp\left[-\frac{E_{pre}}{RT_f}\right][C_{fu}]^a[C_O]^b \tag{52}$$

where $[C_{fu}]$ and $[C_O]$ are the concentration of the fuel and molecular oxygen, respectively, and the exponents $a$ and $b$ are at present taken to be unity. The collision frequency $A_{pre}$ and the activation energy $E_{pre}$ need to be modeled for each fuel. This model is similar to the one proposed by Krazinski et al. (1989). The species molar concentration, $[C_{fu}]$, can be rewritten in terms of the mass fraction by using the relation $[C_{fu}] = \rho_f(Y_{fu})/(M_{fu})$, where $M_{fu}$ is the molecular weight of the fuel species. Thus, Equation (52) can be rewritten in terms of the k-th species mass fraction as

$$\rho_f\left[\frac{\partial Y_k}{\partial t} + u_{f_i}\frac{\partial Y_k}{\partial x}\right] = \nabla\cdot(\rho_f D_k \nabla Y_k) + M_k(P_{Y_k} - L_{Y_k}) \tag{53}$$

Here, Fick's law of species diffusion, i.e., $u_{f_{k_i}} = -(D_k/Y_k)\nabla Y_k$, has been employed and the mixture mass conservation equation has been used. Also, $D_k$ is the diffusion coefficient for the k-th species in the bulk fuel. To solve this equation, the diffusion coefficient must be known for all the species in the bulk fuel. Currently available data on $D_k$ for the fuel is very limited, and no such data is available for the deposit precursor. Specially designed experiments will be required to determine the diffusion coefficients.

The production of the deposit precursor is at the expense of the fuel and oxygen in the bulk phase. Thus, the destruction of the fuel and oxygen species in the bulk fuel is directly proportional to $P_{Y_{pre}}$ such that

$$P_{Y_{fu}} = -\alpha_{fu} P_{Y_{pre}} \tag{54}$$

and

$$P_{Y_O} = -\alpha_O P_{Y_{pre}} \tag{55}$$

where $\alpha_{fu}$ and $\alpha_O$ are coefficients that are functions of the molecular weights $M_k$ and the exponents in the reaction rate ($a$ and $b$) in Equation (52).

In addition to the production of the deposit precursor in the bulk fuel, there will be a loss of the precursor when it is (a) transported to the wall and undergoes phase transition into solid deposits, (b) directly converted into solid deposits in the bulk fuel itself (pseudofluid mass source $\sigma_p$), and (c) when the liquid deposit precursor is converted into a fuel-soluble product that no longer has the tendency to form deposit and is lost from the deposition process. At present, due to lack of detailed understanding of these loss mechanisms, the above three mechanisms are modeled by a single loss term, $L_{Y_{pre}}$, which represents the overall loss of the deposit precursor from the bulk fuel. Similar to the earlier study (Krazinski et al., 1989), we describe this loss term by another Arrhenius term with a different collision frequency $B_{pre}$ and activation energy $E_L$ such that

$$L_{Y_{pre}} = B_{pre} \exp\left[-\frac{E_L}{RT_f}\right] \left[C_{pre}\right]^c \tag{56}$$

Again, $B_{pre}$ and $E_L$ both have to be calibrated for a given fuel, and $c$ is the exponent which for simplicity we choose at present to be unity. Note that the loss term is only present for the deposit precursor, since there is no such mechanism for the fuel and the dissolved oxygen. Thus,

$$L_{Y_{fu}} = L_{Y_O} = 0 \tag{57}$$

### 3.4.2 Reduction of the Model for the Phase I Study

Since we are at present studying a reduced model, we again make some simplifications. We first assume that the fuel and dissolved oxygen can be lumped together into a single species (species $fO$) so that only two species have to be modeled rather than three. By mass conservation, $Y_{fO} + Y_{pre} = 1$; therefore, only one species transport equation has to be solved. We therefore solve the conservation of the deposit precursor species ($Y_{pre} = Y$) with the axisymmetric assumption so that the conservation equation for $Y$ can be written as

$$\rho_f \left[\frac{\partial Y}{\partial t} + u_f \frac{\partial Y}{\partial x}\right] = \frac{\partial}{\partial x}\left[\rho_f D_Y \frac{\partial Y}{\partial x}\right] + \frac{1}{r}\frac{\partial}{\partial r}\left[\rho_f D_Y \frac{\partial Y}{\partial r}\right] + P_Y - L_Y \tag{58}$$

where the production and loss terms are given by

$$P_Y = \rho_f(1-Y)A_Y \exp\left[-\frac{E_P}{RT_f}\right] \tag{59}$$

and

$$L_Y = \rho_f Y B_Y \exp\left[-\frac{E_L}{RT_f}\right] \tag{60}$$

Here, we have assumed that the molecular weights of the fuel+dissolved oxygen and the deposit precursor are the same. As noted above, the solution of this equation requires that the parameters $A_Y$ and $B_Y$ as well as the activation energies $E_P$ and $E_L$ must be calibrated. The calibration process will again depend on the availability of detailed experimental data. Equation (58) is solved subject to proper boundary conditions.

The boundary conditions for the liquid deposit precursor in the fluid phase are

$$\begin{aligned} \frac{\partial Y}{\partial r} &= 0 && \text{at } r = r_3 \\ Y &= 0 && \text{at } x = 0 \\ \frac{\partial Y}{\partial x} &= 0 && \text{at } x = l \end{aligned} \tag{61}$$

The boundary condition at $r = r_2$ is very important. As mentioned earlier, this boundary condition will determine the diffusion/entrainment process occurring at the edge of the deposit layer.

The current lack of understanding of the conversion process and of the mechanism that affects the entrainment process precludes the development of a complex boundary condition at the deposit edge. Most likely, the entrainment of the liquid deposit, and possibly the solid deposit, back into the flowing fuel would be in some manner related to the turbulence levels at the deposit edge and the surface turbulent shear stresses. Since at present we are not solving the turbulent process, we will not attempt to formulate any entrainment process. As a first approximation, we may assume that almost all the precursor deposit that reaches the edge of the solid deposit will convert in some manner to the solid phase. Thus, we must determine the value of $Y$ at $r = r_2$. Making use of the governing form of the conservation equation, we assume that near the edge of the solid deposit layer, the convective motion due to the velocity and the diffusion process can be considered negligible so that at $r = r_2$ we may obtain the boundary condition

$$\rho_f \frac{\partial Y}{\partial t} = P_Y - L_Y \tag{62}$$

Thus, we solve this time-dependent equation at the solid deposit edge with the initial condition at $t = 0$ and $Y(r = r_2) = 0$. The solution of this equation then gives the required boundary condition at the edge of the solid deposit on the wall.

### 3.5 Formation of Deposit Due to Fuel Degradation Reactions

The fuel deposit will form due to the degradation reactions that occur when the fuel is heated. As noted earlier, there are three possible mechanisms that will contribute to the growth of the deposit layer on the heated wall: (a) the surface catalytic reaction, (b) the transport and phase change of the deposit precursor formed in the bulk fuel, and (c) the transport and impaction of the solid deposit formed in the bulk fuel. The net result of these mechanisms will be the growth of the deposit on the metal surface. In the present formulation, we define the thickness of the solid deposit on the wall as the basic parameter. If $\rho_d$ is the density of the deposit, then $\rho_d h = \rho_d(r_2 - r_1)$ will be the net deposit formed per unit area on the heated metal surface.

The final result of the fuel degradation process is the formation of a thin layer of deposit on the metal surface of the heating rod. The dimensional thickness of the deposit, $h = r_2 - r_1$ is a variable in the deposit formation process and can be modeled by

$$\frac{dh}{dt} = A_w \exp\left[-\frac{E_w}{RT_w}\right] + \left[\frac{dh}{dt}\right]_Y + \left[\frac{dh}{dt}\right]_D \qquad \text{at } r = r_2 \tag{63}$$

where $T_w$ is the wall temperature and the first term models the surface catalytic conversion by an activation energy $E_w$. Note that $A_w$ has the unit of velocity. Both $A_w$ and $E_w$ must be calibrated for a given fuel. The modeling of the surface catalytic process by the single Arrhenius rate equation is a major simplification of the complex degradation process. At present it is not clear how the surface catalytic process will degrade the fuel and result in the formation of the solid deposit. Due to lack of proper experimental data on this process, the current model uses a simplified process to simulate the effect of the hot wall on the deposit formation rate. Furthermore, since the wall temperature is nearly the same (i.e., a weak function of time), the calculation of the deposit growth using the surface catalytic reaction [assuming the other two terms in Equation (63) are zero] would result in a *linear* growth of the deposit with time. However, experimental data (Marteney, 1988; Marteney and Spadaccini, 1986) indicate that the overall deposition rate on the wall is *nonlinear* with time and in fact suggests that the growth rate increases with time. This nonlinearity may be due to a more complex catalytic reaction mechanism at the wall. Again, lack of experimental data makes it difficult to determine if this is the mechanism.

The second term models the overall deposition due to the fluid transport of the deposit precursor to the wall. As a first approximation, we may assume that the growth of the deposit near the wall will be in some manner proportional to the loss of the deposit precursor from the bulk fuel, i.e., $dh_Y \propto L_Y$, where $L_Y$ is given by Equation (60).

Neglecting for the moment the third mechanism, the total deposition process can then be modeled by

$$\frac{dh}{dt} = A_w \exp\left[-\frac{E_w}{RT_w}\right] + B_w \Delta L_Y \tag{64}$$

Here, $B_w$ is a dimensionless number that may or may not be a constant, and $\Delta$ is a characteristic length scale within which the phase change from the liquid precursor to the solid deposit would occur. For lack of data, we assumed that this length scale is equal to the grid scale $\Delta r_2$ near the edge of the deposit. Computations using this model indicated that the resulting growth is not much different from the linear growth predicted by the first term alone. Using the JFTOT data (UTC, 1988), a series of

computations was carried out to see how the nonlinearity could be modeled in the growth mechanism. It was then determined that the nonlinear growth mechanism can be fitted to the experimental data by three possible modifications to the above equation. The first modification would be to rewrite Equation (64) as

$$\frac{dh}{dt} = (A_w + a_w t)\exp\left[-\frac{E_w}{RT_w}\right] + B_w \Delta L_Y \tag{65}$$

where $a_w$ is another adjustable constant with the units of acceleration. However, this modified model appeared to have no physical significance other than the possibility that the surface catalytic reaction changes with time. Since there is no data to support this mechanism, it was eventually discarded.

It was then decided to look for the nonlinearity by considering the modification to as a function of the deposit thickness itself. This led to the second modified model:

$$\frac{dh}{dt} = A_w\left[1 + a_{w_1}\sqrt{\frac{h}{h^*}}\right]\exp\left[-\frac{E_w}{RT_w}\right] + B_w \Delta L_Y \tag{66}$$

Here, $a_{w_1}$ is again a constant with the unit of velocity; fitting the model to the data resulted in a value of $a_{w_1} \approx 2A_w$. The term $h^*$ is a reference value for the deposit thickness which is approximated as follows: As the deposit grows, there may be a critical thickness beyond which the deposit growth will affect the heat transfer process. At this limit, we may approximate the heat balance at $r = r_2$ as

$$\kappa_d \frac{\Delta T_d}{h^*} \approx \kappa_f \frac{\Delta T_f}{\delta_{th}}$$

where $\Delta T_d$ and $\Delta T_f$ are, respectively, the temperature difference in the solid deposit and in the bulk fuel. Here, $\delta_{th}$ is the thickness of the thermal boundary layer above the deposit. This then gives

$$h^* \approx \frac{\kappa_d}{\kappa_f}\delta_{th}\left[\frac{\Delta T_d}{\Delta T_f}\right] \tag{67}$$

If we further assume $\Delta T_d \approx \Delta T_f$, Equation (67) then gives a rough estimate for $h^*$. Note that the assumption $\kappa_d = A_d \kappa_f$, where $A_d < 1$, implies $h^* \approx A_d \delta_{th}$. Using $h = h^*$ in Equation (66), we find the characteristic time scale to reach the critical thickness as

$$t^* \approx \frac{h^*}{\left[A_w\left[1 + a_{w_1}\right]\exp\left[-\frac{E_w}{RT_w}\right] + B_w \Delta L_Y\right]}$$

The model equation (66) appears to have some significance in that the nonlinear correction to the surface catalytic reaction may be a result of the fact that the surface reaction mechanism may be modified by the growth of solid deposit on the wall. Comparing Equations (65) and (66), we note that both these models can be considered equivalent if we assume that for the nonlinear growth, the deposit thickness $h \propto t^2$. However, since there is no experimental data to validate this possible mechanism, we were unable to formulate a physical process that would be consistent with the $\sqrt{h}$ variation for the nonlinear process.

After some additional consideration, we determined that the nonlinear term could also be modeled by a third mechanism, which can be expressed by

$$\frac{dh}{dt} = A_w \exp\left[-\frac{E_w}{RT_w}\right] + B_w \Delta \sqrt{\frac{h}{h^*}}\, L_Y \tag{68}$$

This mechanism assumes that the nonlinear growth of the deposit is in some way related to the deposition process associated with the phase change of the liquid precursor in the bulk fuel into solid deposit near the wall. After some theoretical considerations, we eventually formulated a possible explanation for this mechanism, which is discussed below.

There is experimental evidence that the deposition process is not uniform in space and in fact could result in a complex shape of the deposit surface. There is also some evidence that the solid deposit is initially very porous. Figure 2 shows the local surface of a deposit, indicating that there may be regions with "holes" into which the bulk fuel and the liquid deposit precursor may be entrained. In the regions where the thickness is small, the bulk fuel will be in contact with the hot wall and the surface reaction mechanism will result in a locally larger deposition rate. This mechanism may eventually (after a long time) equilibrate and a uniformly thick solid deposit would form on the heated surface. However, the initial surface undulations may be a consequence of a process in which the liquid deposit precursor in the bulk fuel undergoes a phase change into solid deposit near the wall and randomly falls and adheres to the metal surface. Thus, in general, at any given time we have an "average" deposit thickness defined as $\langle h(x, t)\rangle$ and the variance of $h$ given by $\eta_h(x, t)$.

We then assume that

$$\frac{d\langle h\rangle}{dt} \propto \eta_h \tag{69}$$

This equation implies that the growth of the average deposit thickness with time will increase with the increase in the variance or the extent of nonuniformity. Since we are assuming that the nonuniformity of the deposit is a result of some random process, we can assume that this random process can be modeled as a Gaussian distribution. If $P$ is the probability density function that defines the probability of finding the thickness within the range $h$ and $h + dh$, then by definition

$$\begin{aligned} \langle h\rangle &= \int P\, h\, dh \\ \eta_h^2 &= \int P \left[h - \langle h\rangle\right]^2 dh \end{aligned} \tag{70}$$

We now need to define the probability density function in terms of the Gaussian distribution. We assume that

$$P = \ln\left[\langle h\rangle\right] G \tag{71}$$

where $G$ is the Gaussian probability distribution. By definition, the Gaussian distribution satisfies

$$\int G dh = 1 \tag{72}$$

and

$$\begin{aligned} \langle h\rangle &= \int G h dh \\ \eta_h^2 &= \int G \left[h - \langle h\rangle\right]^2 dh \end{aligned} \tag{73}$$

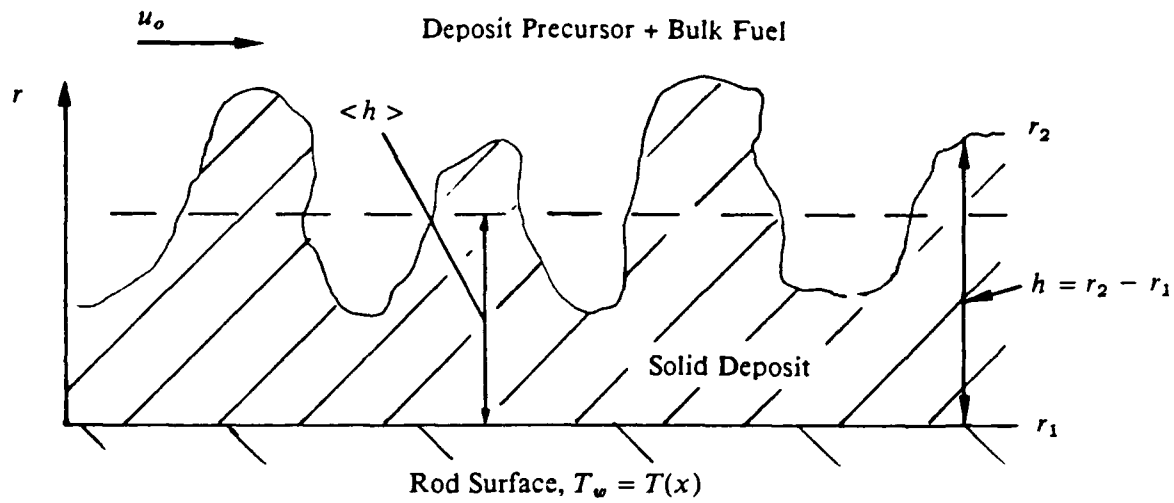


**Figure 2. Local Deposit Surface Nonuniformities Due to Random Deposition**

It can be shown that this definition satisfies Equation (70) by considering the time derivative of Equation (73) as

$$\frac{d\langle h\rangle}{dt} = \frac{d}{dt}\int Phdh = \int \frac{dP}{dt}hdh \tag{74}$$

Using the definition of $P$ from Equation (71), we can easily show that Equation (74) is an identity, i.e., the right-hand side becomes the same as the left-hand side. If we follow the same procedure and compute the first time-derivative of the variance, $\eta_h^2$, we obtain

$$\frac{d}{dt}\eta_h^2 = \frac{d}{dt}\int P\left[h - \langle h\rangle\right]dh = \frac{1}{\langle h\rangle}\frac{d\langle h\rangle}{dt}\eta_h^2 \tag{75}$$

Integrating Equation (75) results in

$$\eta_h^2 = \beta^2\langle h\rangle$$

or

$$\eta_h = \beta\sqrt{\langle h\rangle} \tag{76}$$

Thus, by Equation (68), we obtain

$$\frac{d\langle h\rangle}{dt} \propto \eta_h \approx \beta\langle h\rangle^{\frac{1}{2}} \tag{77}$$

Here, $\beta$ is a constant of the order of unity. Thus, the nonlinear term in Equation (67) can be related to the random deposition process near the wall by virtue of Equation (77).

Finally, in Equation (63), we had identified a third possible mechanism for the growth of the solid deposit layer on the wall. This mechanism is related to the solid particles formed in the bulk fuel when the liquid precursor condenses into solid particles. These solid particles will then migrate towards the wall and, upon reaching the wall, will begin to adhere to it. Note that this mechanism is different than the mechanism for $(dh/dt)$ discussed earlier. In that model, Equation (68), the additional solid deposit formed on the wall is the result of the phase change of the liquid precursor into solid deposit *near* the deposit surface. Diffusion through the bulk fuel is not important for this mechanism. For the third mechanism, however, the migration of the solid deposit formed in the bulk fuel towards the wall is important. This migration and subsequent adhesion process needs to be modeled because it will contribute to the overall deposition rate. Here we use as a first approximation the approach used in aerosol deposition theories (Davies, 1987) and formulate the third mechanism as a function of a diffusion coefficient and the normal gradient of the volume fraction of the solid particles in the bulk fuel. Thus,

$$\left[\frac{dh}{dt}\right]_D = C_w^* D_{sp}\frac{\partial\lambda}{\partial r} \tag{78}$$

where $D_{sp}$ is the diffusion coefficient for the solid particles, $C_w^*$ is an adjustable constant of the order of unity, and the equation is valid at $r = r_2$. From aerosol deposition theory, we estimate the diffusion coefficient in terms of the vertical velocity fluctuation and a characteristic length scale. Thus,

$$D_{sp} = v_r'\Delta \tag{79}$$

where the vertical velocity fluctuation near the deposit edge is given by

$$v_r' = f_1 u^* Sc^n \tag{80}$$

In Equation (80), $f_1$ is a constant and $u^*$ is the friction velocity, usually given as $u^* = \sqrt{(\tau_w/\rho)}$. Typically, $u^*$ is a small fraction of the free stream velocity, $u_o$, i.e., $u^* \approx f_2 u_o$, where $f_2 \approx 0.01-0.05$. Here, $\tau_w = \mu_w(\partial u/\partial r)$ is the shear stress at the edge of the deposit ($r = r_2$). Also, $Sc = \nu/D_{sp}$ is the Schmidt number and $n$ is an exponent. The value of $f_1$ and $n$ depends in part on the state of the wall, i.e., for smooth walls, aerosol deposition data indicates $f_1 = 0.075$ and $n = -2/3$; for rough walls, $f_1 = 0.08$ and $n = -1/2$. For the present study, the rough wall assumption is probably more appropriate and thus is employed here. The value of the Schmidt number is typically in the range of $10^6$ for very small particles. Therefore, for the present study we used $n = -2/3$, $f_1 = 0.08$, and $Sc = 10^6$.

In the Phase I model, we had assumed that there is no solid deposit present in the bulk fuel. Thus, Equation (78) cannot be used for the third mechanism directly. An indirect way to implement this mechanism is to rewrite Equation (78) as

$$\left[\frac{dh}{dt}\right]_D = C_w D_Y \frac{\partial Y}{\partial r} \qquad \text{at } r = r_2 \tag{81}$$

where $C_w$ is another adjustable constant of the order of unity and $D_Y$ is the diffusion coefficient for bulk fuel precursor near the deposit edge, which is assumed to be the same as $D_{sp}$. This mechanism essentially indicates that the normal diffusion of the liquid precursor formed in the bulk fuel towards the wall will result in an additional growth in the solid deposit. However, the liquid precursor can only become solid deposit by undergoing a phase change. Thus, if the temperature near the solid deposit surface is high, the liquid deposit precursor will not solidify and instead will form a liquid boundary layer flowing in the downstream direction on top of the solid deposit. This liquid layer will start to solidify only if the temperature drops below a critical point, characteristically the condensation temperature. Therefore, we make an additional restriction that the third mechanism contributing to the deposit growth, Equation (81), will be negligible if $\Delta T = T_w(x) - T_w(x - \Delta x) \geq 0$, i.e., the temperature is increasing in the downstream direction, and $(dh/dt)_D \neq 0$ only if $\Delta T < 0$, i.e., the fuel temperature at $r = r_2$ starts to decrease in the outflow direction. At present, this modified formulation, although reasonable, cannot be fully validated. Therefore, in the discussion of the results later in this report, no major emphasis is placed on this model.

This completes the formulation of the system of differential equations that governs the five unit processes involved in the fuel degradation and deposit formation process. These unit processes are coupled through the boundary conditions at the interfaces. If detailed data were available, it would be worthwhile to evaluate the validity of the full model formulated here. In the reduced model for the Phase I investigation, no solid particles are assumed to be present in the bulk fuel. The velocity field is assumed known, and the transport of heat is a passive scalar transport process. The solid phase can be added in a subsequent study if further data is available for validation. The parameters in the present model are the thermal conductivities of the heating element and the deposited material, the activation energy and rate constants for the surface catalytic reaction and the fluid phase reaction, and the viscosity and thermal conductivity of the bulk fuel. The operating parameters are the dimensions of the apparatus, the flow rate of the fuel, and the heat flux into the heating element.

## 4. THE NUMERICAL CODE

The reduced mathematical model of the fuel degradation problem, as described in the previous section, was implemented in a numerical code to carry out a series of simulations. For the eventual development of a general purpose thermal prediction code, we undertook the task of developing a completely new CFD code for this problem. The numerical method used is described below.

In the Phase I research, the fluid was assumed to be JP-5 with prescribed transport properties, i.e., $\rho_f(T)$, $c_{p_f}(T)$, $\kappa_f(T)$, $\mu_f(T)$, and with a known flow velocity. Thus, the fluid dynamics is entirely decoupled from the heat exchange problem. The velocity profile for a flow in an annular tube can be obtained exactly from classical considerations (Landau and Lifshitz, 1987) as

$$u_f(r) = \frac{\Delta p}{4\mu_f l}\left[r_3^2 - r^2 + \frac{r_3^2 - r_2^2}{\log\left[\frac{r_3}{r_2}\right]}\log\left[\frac{r}{r_3}\right]\right] \tag{82}$$

where $\Delta p$ is the imposed pressure gradient, $r_3$ is the outer radius, and $r_2$ is the inner radius, which in the present case of deposit growth would be $r_2 = r_2(x,t)$. Also, $l$ is the length of the tube and $\mu_f$ is the kinematic viscosity of the fluid. Strictly speaking, if $r_2 = r_2(x,t)$ for the cases with deposit growth, then $u_f$ will vary with $(x,t)$. In that case, the velocity profile at each axial location and at each time step can be modified to take this into account.

The heat transfer in the rod, Equation (2), the heat transfer across the deposit, Equation (9), and the heat balance in the fuel, Equation (44), were solved using both an explicit time-marching scheme and an implicit ADI scheme. To achieve high accuracy, a high-order spatial discretization scheme was developed. Steady-state temperature fields without deposit growth were calculated using both schemes.

### 4.1 The Explicit Scheme

The explicit scheme consists of a high-order compact scheme (the Padé approximation scheme) from which a formally fourth-order-accurate scheme can be obtained by using a compact stencil. If we denote $\delta_o u_j = (u_{i+1} - u_{i-1})/2\Delta x$ as the second-order-accurate central difference for the first spatial derivative and $\delta^2 = (u_{i+1} - 2u_i + u_{i-1})/\Delta x^2$ as the second-order-accurate second derivative, then by Taylor series we have

$$\delta_o u_j = \frac{du}{dx} + \frac{\Delta x^2}{6}\frac{d^3u}{dx^3} + O(\Delta x^4) \tag{83}$$

Thus, the first derivative can be written from Equation (83) as

$$\frac{du}{dx} = \left[1 + \frac{1}{6}\delta^2\right]^{-1}\frac{u_{i+1} - u_{i-1}}{2\,\Delta x} \tag{84}$$

where $\delta^2$ is the central second difference operator. This discretization is on a uniform grid. Extension to a nonuniform grid is straightforward. To solve this equation, a tridiagonal system must be inverted. Also, since specific boundary conditions are prescribed in the present case, special consideration must

be given to the discretization at the boundaries. Instead of the central differences, we employ one-sided second-order difference near the boundaries so that

$$\frac{-3u_0 + 4u_1 - u_2}{2\Delta x} = \frac{du_0}{dx} - \frac{\Delta x^2}{18} + O(\Delta x^4) \tag{85}$$

This spatial discretization was combined with the Runge-Kutta time-stepping scheme to produce a highly accurate unsteady scheme. The scheme developed in this study was written so that spatial and temporal accuracy of up to fourth-order could be obtained. A second-order-accurate scheme was also developed in this study.

Fourth-order compact schemes can have problems due to numerical instability in flows with sharp gradients. Both second- and fourth-order schemes were implemented and were then compared using simple test problems. For one-dimensional wave motion with periodic boundary conditions, it was determined that, with the compact scheme, only six grid points are required to resolve the wave reasonably without significant phase errors, whereas the second-order scheme required a much higher resolution. For the present configuration with a constant heat flux into an initially cold rod and fuel, the initial sharp temperature gradient (at $t = 0$) caused numerical instability when the fourth-order scheme was used. When the initial temperature distribution in the rod and in the bulk fuel was more uniform, the compact scheme encountered no major instability. Thus, it appeared that the best approach would be to begin the computation using the second-order scheme and then switch to the higher-order scheme once the temperature field in the rod and in the fuel has developed. For the reduced model used in Phase I, both the second- and fourth-order schemes resulted in identical steady states. Since the computational overhead for the second-order scheme was significantly lower, most of the steady-state computations employed the second-order scheme.

### 4.2 The Implicit Scheme

The basic problem with the explicit scheme is that the stability considerations severely limit the time step for the heat conduction equation to very small steps, which leads to excessive computational cost. To avoid this restriction on the time step, we implemented an implicit scheme based on the alternate direction implicit (ADI) scheme. Such schemes are well known and have been extensively used in the study of such problems where the time step restriction can be quite stringent. We will not go into the details of this scheme since it is described thoroughly in many textbooks (Anderson et al., 1984). Here we briefly summarize the main steps. Consider a general equation of the form

$$\frac{\partial \phi}{\partial t} = a\phi_{xx} + b\phi_x + c\phi_{rr} + d\phi_r \tag{86}$$

where $a$, $b$, $c$, and $d$ need not be constant and in the present case are assumed to be functions of $\phi$. Here, $\phi$ may be considered to represent the temperature, $T$. Also, the subscripts indicate differentiation with respect to $x$ or $r$; for example, the subscript $xx$ indicates the second derivative of $\phi$ with respect to $x$. Further, we will denote $D_x$ and $D_r$ as the finite difference approximation to the $x$-derivatives and the $r$-derivatives, respectively. Then, using the Crank-Nicholson scheme, we can write

$$\left[I - \frac{\Delta t}{2}D_x - \frac{\Delta t}{2}D_r\right]T^{n+1} = \left[I + \frac{\Delta t}{2}(D_x + D_r)\right]T^n + O(\Delta t^2) \tag{87}$$

Using approximate factorization, we obtain

$$\left[I - \frac{\Delta t}{2} D_z\right]\left[I - \frac{\Delta t}{2} D_r\right] T^{n+1} = \left[I + \frac{\Delta t}{2} D_z\right]\left[I + \frac{\Delta t}{2} D_r\right] T^{n} \tag{88}$$

In the present case, since the coefficients in Equation (86) are functions of $\phi$, we make the simplifying assumption that the coefficients and the boundaries are constant for one time step. This reduces the time-accuracy to $O(\Delta t)$ but will not affect the solution if only steady-state solutions are required.

We solve this equation in the rod using the Peaceman-Rachford ADI scheme (Peaceman and Rachford, 1955) as follows

$$\left[I - \frac{\Delta t}{2} D_z\right] \tilde{T}^{n+1/2} = \left[I + \frac{\Delta t}{2} D_r\right] T^{n} \tag{89}$$

$$\left[I - \frac{\Delta t}{2} D_r\right] T^{n+1} = \left[I + \frac{\Delta t}{2} D_z\right] \tilde{T}^{n+1/2} \tag{90}$$

A similar scheme was used to solve for the temperature in the fluid; in this case the convection term was added into the $x$-operator. A modification of this type was used by Polezhaev (1967). Since in each time step the coefficients are changing, we linearized locally and assumed that the coefficients and boundary conditions remained constant during each time step. After a complete time step, the coefficients and boundary conditions were updated. This reduced the total accuracy to $0(\Delta t, \Delta x^2)$.

Since there is a convective term in the present case due to the velocity field, this scheme will not be unconditionally stable; however, the time step restriction with dependence on $\Delta x$ for the implicit scheme is still much larger than the time step possible with the explicit scheme (Anderson et al., 1984). All the steady-state results presented in this report employed the implicit scheme.

## 5. RESULTS AND DISCUSSION

In this section, we describe the results of the study. Before describing the results, it is important to emphasize that there were quite a few variables that had to be calibrated for the deposition process. We essentially assumed that the data on the JFTOT could be used for this purpose. However, the data itself was quite sparse and there were many parameters that were still unknown. Therefore, although the model developed in the present study appears to have the proper physics to simulate the deposition formation and the growth of the solid deposit on the wall, the full evaluation of the model will require additional data on the physical processes involved.

The JFTOT data used here (UTC, 1988) for calibration had three distinct features. The first was that the measured wall temperature on the JFTOT was not uniform and in fact had a peak at a fixed axial location. After some initial computations, it became quite clear that, with a constant heat flux boundary condition at the centerline, the computed temperature of the wall did not have the variation observed in the JFTOT data. It appears that the peaked temperature distribution on the wall is due to the three-dimensionality of the flow field inside the JFTOT (CRC, 1978; Oh et al., 1989) and to the fact that the fuel outflow region is cooled, so that significant heat loss occurs at the outflow. Since the present configuration is axisymmetric, it was not possible to predict the wall temperature distribution that was observed in the JFTOT experiments by using the constant uniform heat flux conditions. It was possible, however, to mimic the 3D effects by modifying the heat flux condition. This modification is described below. For the calibration studies, however, we decided to use the curve-fitted temperature distribution provided by the sponsor for the wall temperature.

The second feature observed in the JFTOT data (UTC, 1988) was that as the duration of the test increased, the deposition rate also increased. This nonlinear behavior appears to be in agreement with the observations of Marteney (1988). As mentioned earlier, this nonlinear growth data was the primary information used to calibrate the model.

Finally, the third distinct feature observed in the JFTOT experiments was that solid deposit distribution was biased in the downstream direction such that more solid deposit was present downstream of the peak temperature location. Some attempt to model this unusual feature was attempted and is also described here.

The process of model calibration involved first obtaining the steady-state temperature distribution on the rod and in the fluid using the assumption that no deposit was forming. This essentially required the solution of Equation (1) and (44) subject to proper boundary conditions. Since the JFTOT wall temperature distribution could not be reproduced by the present axisymmetric model, we obtained the steady-state temperature field in the bulk fuel by specifying the temperature profile near the centerline of the rod as the boundary condition so that at steady state the wall temperature at $r = r_1$ matches the experimental curve fit. Once the steady-state temperature field in the bulk fuel was determined, we solved the deposit growth equation (68) and the liquid precursor growth equation (62) with the temperature field given by the steady-state field. The effect of deposit growth on the heat transfer process was taken into account by the method described in Section 3.2. The calibration of the data for the given temperature field was then carried out. The results of these studies are summarized here.

The basic JFTOT configuration used in this study had the following dimensions and reference conditions:

$$r_1 = 1.5625 \text{ mm}, \quad r_3 = 2.3125 \text{ mm}, \quad l = 60 \text{ cm}$$

$$u_o = 0.0107 \text{ m/s}, \quad T_o = 293K, \quad \text{Re} \approx 10$$

All other reference properties, such as $\mu_{f\infty}$, $\kappa_{f\infty}$, and $\rho_{f\infty}$, are computed using the curve fit at the inlet temperature, $T_o$. Notice that for the flow speed used here, the Reynolds number is very low; therefore, slow flow (Stokes) approximation could be used to neglect the convective effects. However, we retain the convective terms in our formulation. The low Reynolds number of the flow implies that laminar flow approximation is applicable here.

Steady-state solutions for various boundary conditions were obtained to determine the capabilities of the explicit and implicit numerical schemes. In general, the solutions obtained with the two schemes were nearly identical. Since the implicit scheme is more appropriate for the steady-state calculation, all the results presented here employed the implicit scheme. Furthermore, only characteristic solutions are presented here.

Figure 3 shows the temperature distribution in the rod and in the fuel for the case in which a constant heat flux condition was used near the centerline. For this calculation, 64 grid points in the $x$-direction and 42 grid points in the radial direction (10 points in the rod, 32 points in the fuel) were used, and it was assumed that the rod is insulated at $x = 0$ and $x = l$. A constant heat flux of 400 $kW/m^2$ was used for this calculation. Figure 3a shows the temperature surface plotted such that the fuel inflow temperature was normalized to zero. The constant temperature surface shown in Figure 3a is plotted in the computational plane and thus is not to scale. Figure 3b shows the temperature contours in the rod and in the fuel—again plotted in the computational plane for clarity (since the rod is very long and very thin). In comparing Figures 3a and 3b, we note that there is a temperature boundary layer in the fluid above the rod. Since the fuel at the inlet is cold and is flowing in the positive $x$ direction, it convects the heat downstream so that the fuel temperature is lower near the inlet and the temperature continuously rises towards the outflow. In Figure 3c, the temperature profiles are plotted at various axial locations and the thermal boundary layer is more apparent. Peak temperature is observed near the outflow.

We repeated this calculation (not shown here) with the assumption that there are heat losses at the two ends of the rod. However, there was no major change in the temperature distribution except for a decrease in temperature near the outflow. These two calculations clearly indicated that the constant heat flux boundary condition will not result in a temperature distribution as observed in the JFTOT data. However, the temperature field distribution obtained in these calculations were similar to those observed in the heated tube experiments by Marteney (1988), which showed that the temperature continues to rise toward the outflow region.

These calculations were then repeated with the heat flux modified at the centerline such that it had a parabolic shape with a maximum heat flux at the midpoint of the rod, i.e., $x = 30$ cm. The peak heat flux was adjusted so that the peak wall temperature was near the observed value for a specified JFTOT case (UTC, 1988) with a peak temperature of 287°C (550°F). Figures 4a through 4c show the temperature surface, the temperature contour, and the temperature profiles, respectively, for this calculation. Figure 4a clearly shows that there is a peak in the temperature field near the wall. The temperature contours shown in Figure 4b indicate that, on the wall, the temperature peak is not at $x = 30$ cm where the input was a maximum but rather a small distance downstream of the midpoint location. This is primarily due to the convective effects caused by the fluid flow on the top of the rod. This downstream shift of the peak location is thus consistent with observations in the JFTOT experiments (UTC, 1988). The thermal boundary layer profiles at various axial locations show that downstream of the peak location, the thermal boundary layer thickness decreases since the peak values at

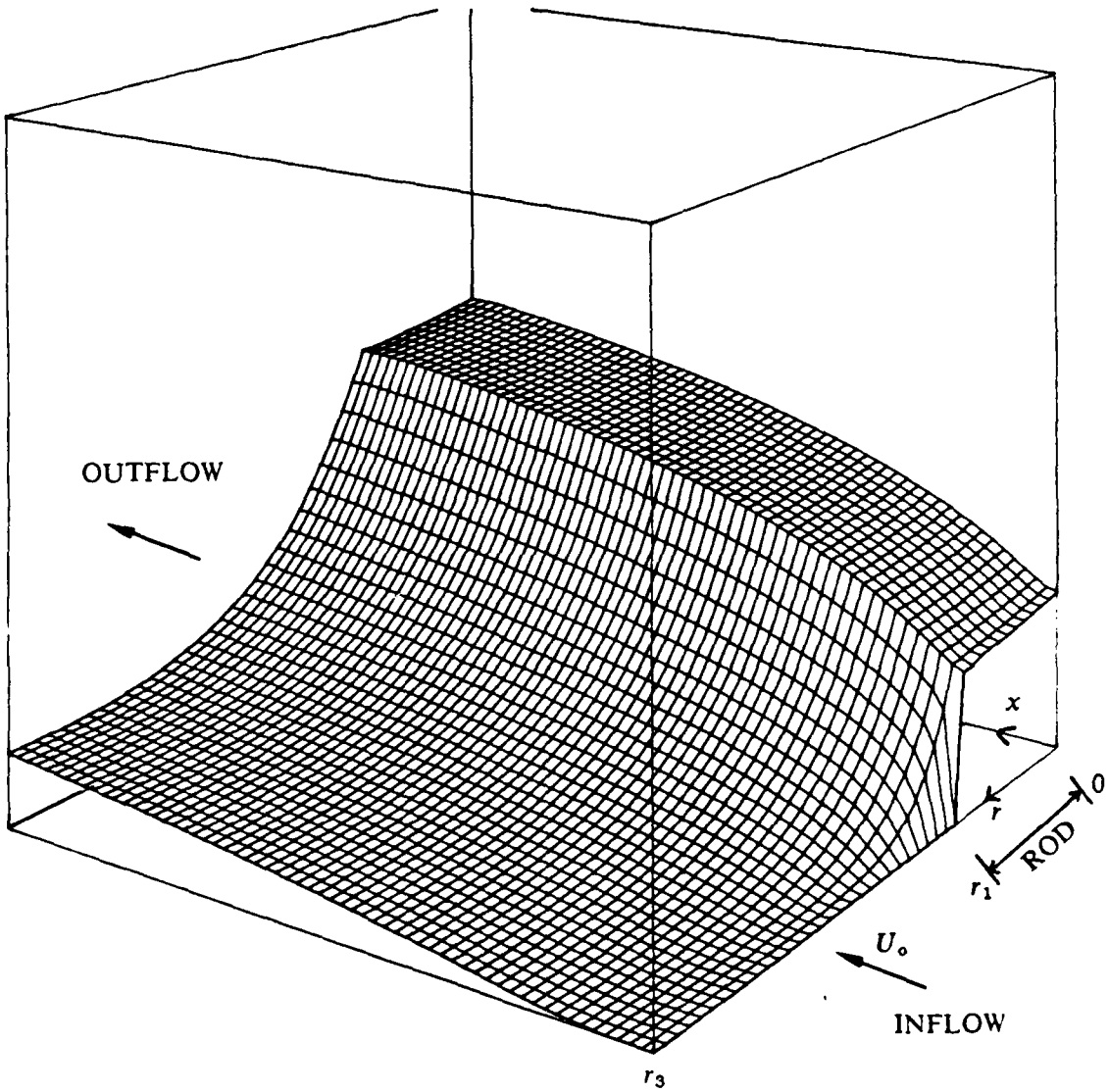


a. Steady-state temperature surface

**Figure 3.** **Steady-State Temperature Field in the Heating Rod and in the Fuel with a Constant Heat Flux Boundary and Insulated Ends**

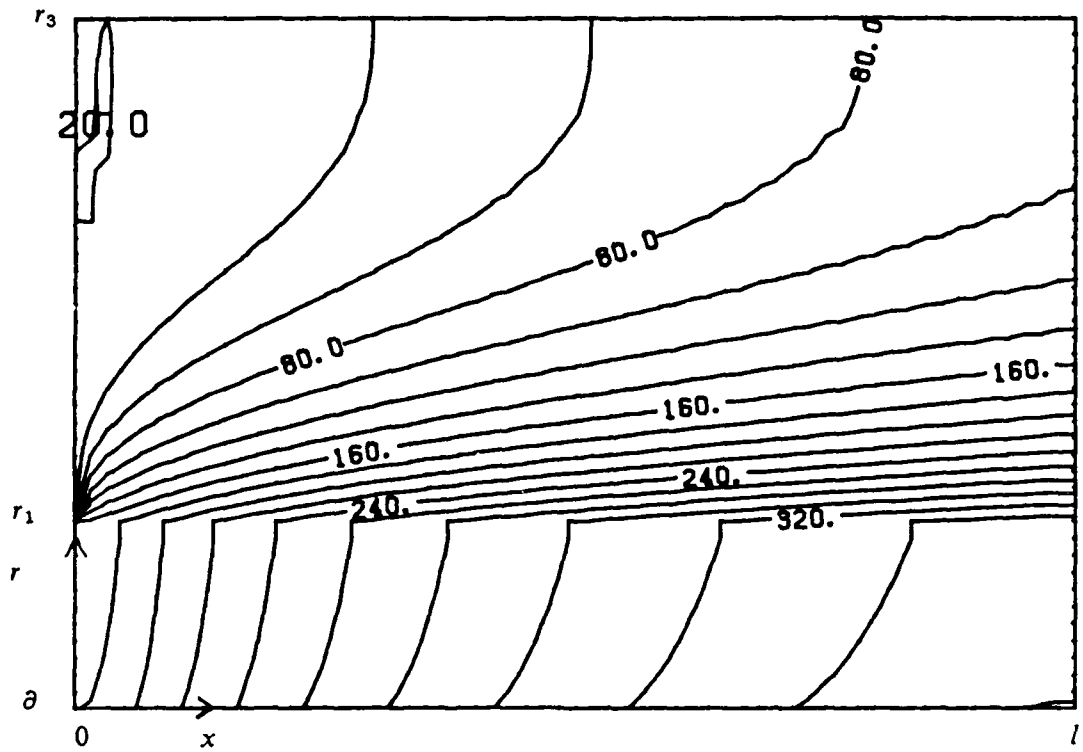


b. Temperature contours in the rod and fuel. Contour interval is 20°C.

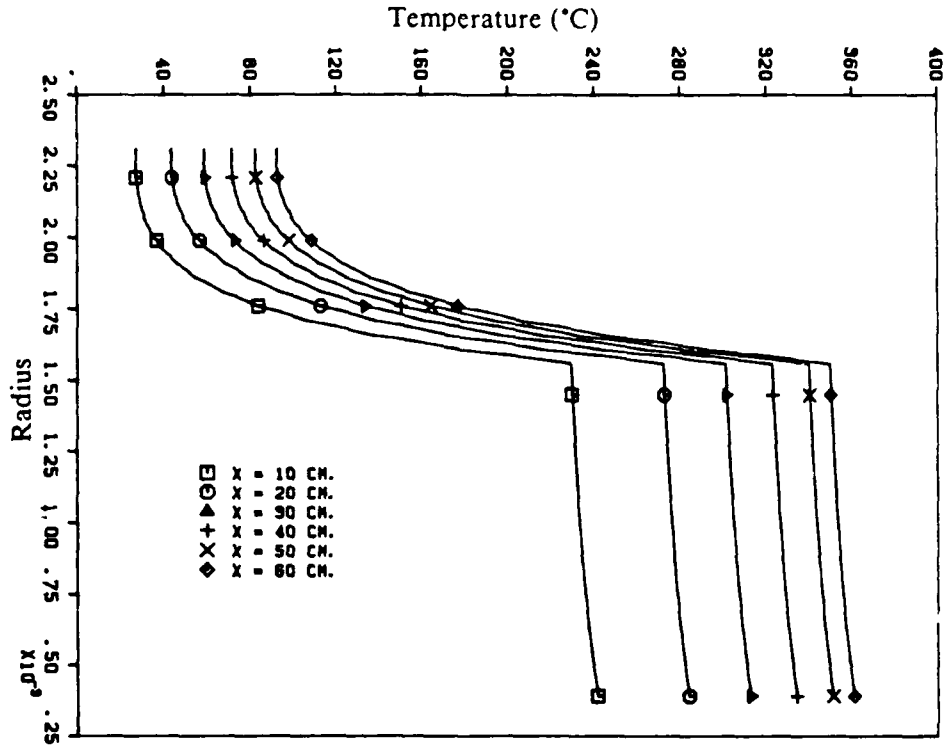


c. Temperature profiles in the rod and fuel at various axial locations

**Figure 3.** **Steady-State Temperature Field in the Heating Rod and in the Fuel with a Constant Heat Flux Boundary and Insulated Ends (Cont.)**

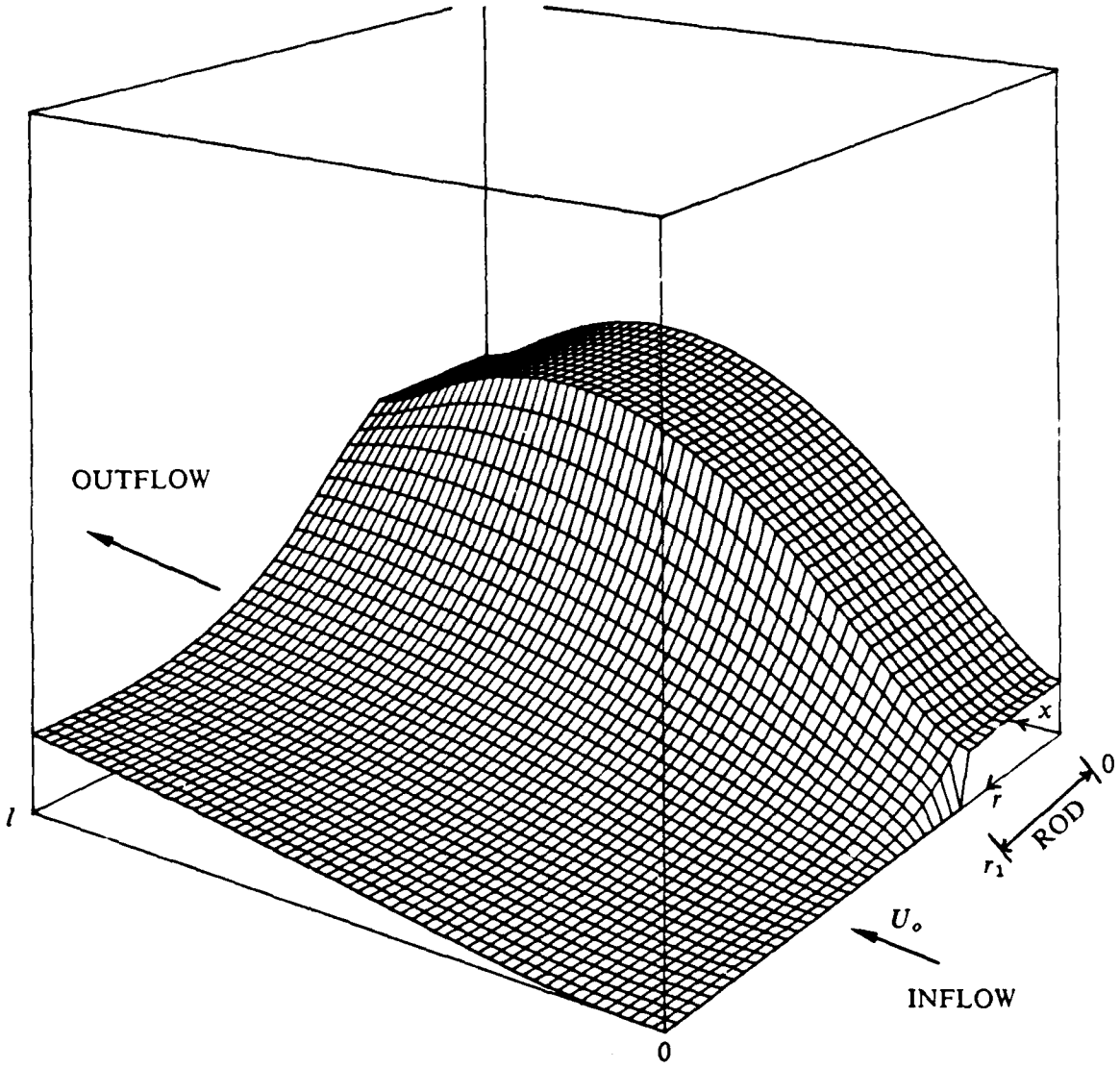


a. Steady-state temperature surface

**Figure 4.** **Steady-State Temperature Field in the Heating Rod and in the Fuel with a Parabolic Heat Flux Boundary and Insulated Ends**

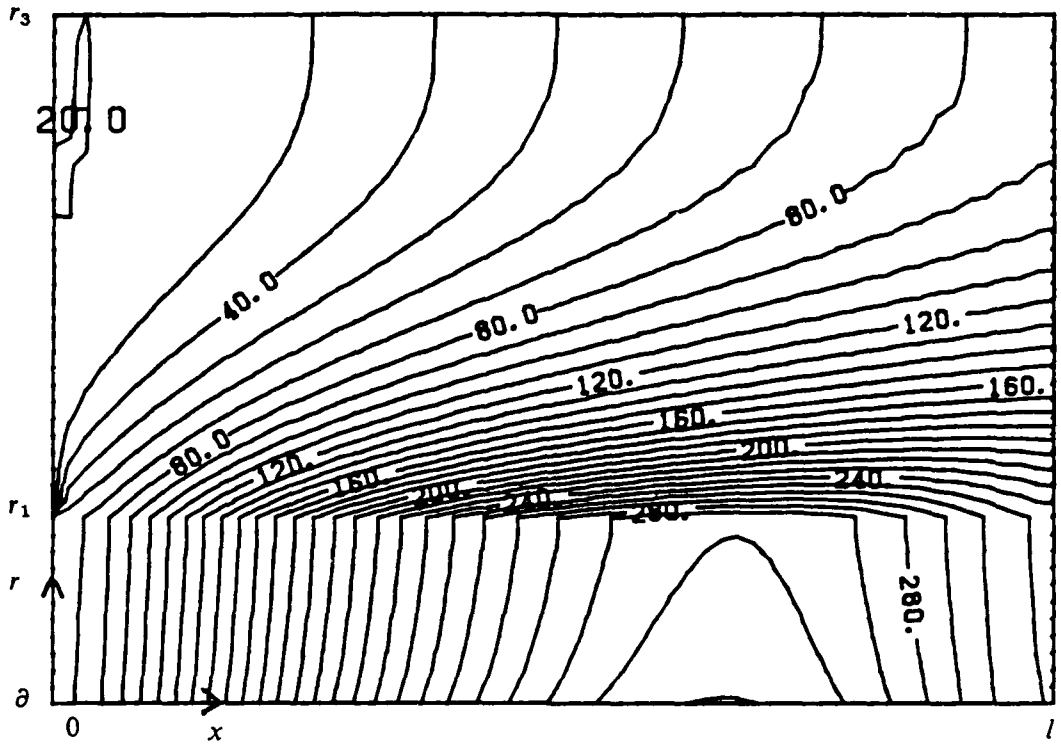


b. Temperature contours in the rod and fuel. Contour interval is 10°C.

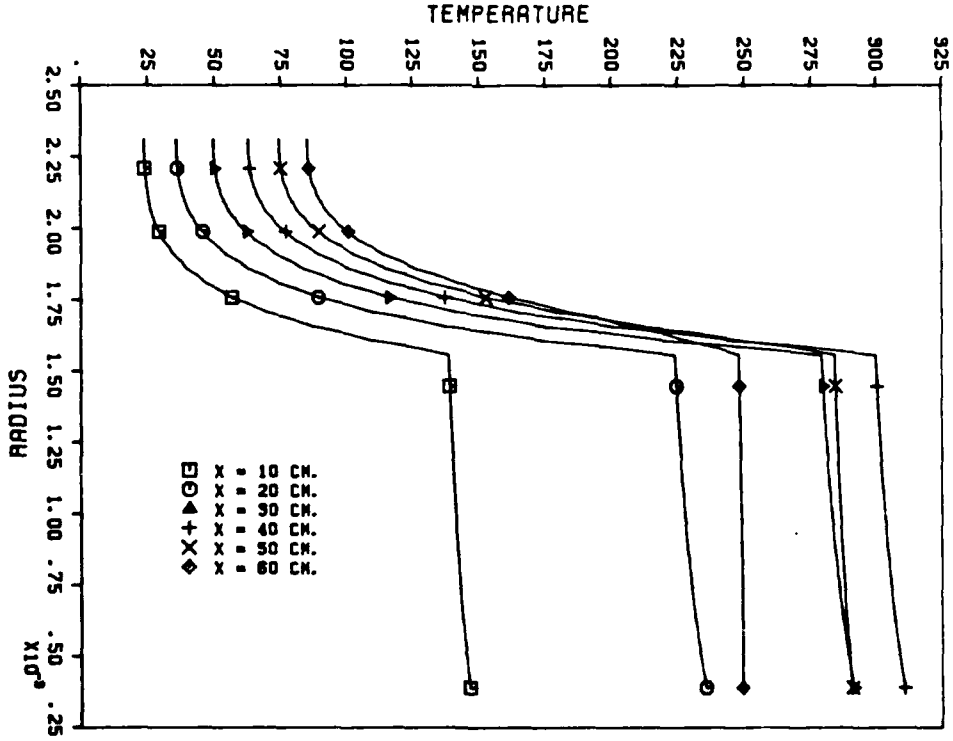


c. Temperature profiles in the rod and fuel at various axial locations

**Figure 4. Steady-State Temperature Field in the Heating Rod and in the Fuel with a Parabolic Heat Flux Boundary and Insulated Ends (Cont.)**

the wall are dropping. With the modified heat flux boundary condition, this calculation essentially mimicked the temperature distribution observed in the JFTOT data. Since the actual JFTOT experimental setup was cooled at the downstream end, we also repeated the above-mentioned calculations with a heat loss at the downstream end (not shown here). No major change in the solution was observed except for a decrease in the temperature as the outflow is reached. These types of boundary heat flux modifications are somewhat arbitrary since the JFTOT flow field is three-dimensional and the current study is axisymmetric.

Subsequently, we decided not to attempt to reproduce the JFTOT wall temperature data using the constant or modified heat flux boundary conditions. Instead, we used the curve fit provided by the sponsor for the wall temperature distribution, of the form

$$T_w(x) = A + Bx + Cx^2 + Dx^3$$

where $A$, $B$, $C$, and $D$ are specified constants. A similar temperature distribution with a modified value for $A$ was imposed near the centerline of the rod at $t = 0$ so that, at steady state, the wall temperature distribution agreed with the experimental curve fit. The steady-state temperature field in the rod and in the bulk fuel was then determined and stored. Since the results were similar to the solution shown above, they are not presented here. Subsequently, the calibration studies were carried out. In the following, we describe some of the more pertinent results of the calibration studies.

To determine the form of the deposit growth equation (68), quite a few parameters had to be determined. For the first mechanism, i.e., the catalytic wall reaction, two parameters had to be determined, $A_w$ and $E_w$. From the JFTOT data (UTC, 1988), it had appeared that the wall activation energy had a value in the range of 35-40 kcal/mole for the types of JP-5 fuel studied. The experimental data for the nonlinear growth of the deposit was for the JP-5 fuel with an activation energy of $E_w = 39$ kcal/mole. We therefore decided to fix the wall activation energy to this value. Thus, the calibration of the linear growth of the deposit due to the catalytic wall reaction required the determination of the collision frequency, i.e., $A_w$.

For the second term, i.e., the nonlinear growth of the wall deposit due to the random impaction and adhesion of the solid particles formed due to phase change of the liquid precursor near the wall, we had to determine the activation energies, $E_p$ and $E_L$, and the collision frequencies, $A_P$ and $A_L$, for the bulk fuel precursor production and loss mechanisms, Equations (59) and (60). We followed the study of Krazinski et al. (1989) and used $E_P = 30$-40 kcal/mole and $E_L = 35$-45 kcal/mole for the model. Most of the results shown here employed $E_P = 30$ kcal/mole and $E_L = 35$ kcal/mole. The constant $B_w$ in Equation (68) was set to unity for lack of any additional experimental information on this mechanism. Then the calibration process required the determination of the constants $A_p$ and $A_L$. The details of all the calibration calculations carried out will not be discussed here; instead, we will focus on some characteristic results.

Figure 5 illustrates the time-dependent growth of the solid deposit on the wall for a variety of choices of the calibration constants. All curves are identified in the figure. With $B_w = 0$ and $C_w = 0$, we obtain the linear growth of the deposit due to the wall catalytic reaction with any value of $A_w$. The calibration study indicated that $A_w = 10^4$ m/s is a good choice. This figure also shows the effect of just the nonlinear second term with $A_w = 10^{-8}$ m/s and $C_w = 0$ by another curve. The nonlinear term allows the deposit to grow very slowly at first and then, when the liquid precursor begins to form in the bulk fuel next to the wall, the nonlinear term rapidly grows in importance. Finally, this figure also shows the effect of combining the various mechanisms for the deposit growth. Comparison with the experimental data shows that values of $A_P = 9\times10^7 \text{sec}^{-1}$ and $A_L = 9\times10^8 \text{sec}^{-1}$ for the chosen values of $E_P$ and $E_L$ appear to provide close agreement with the experimental data.

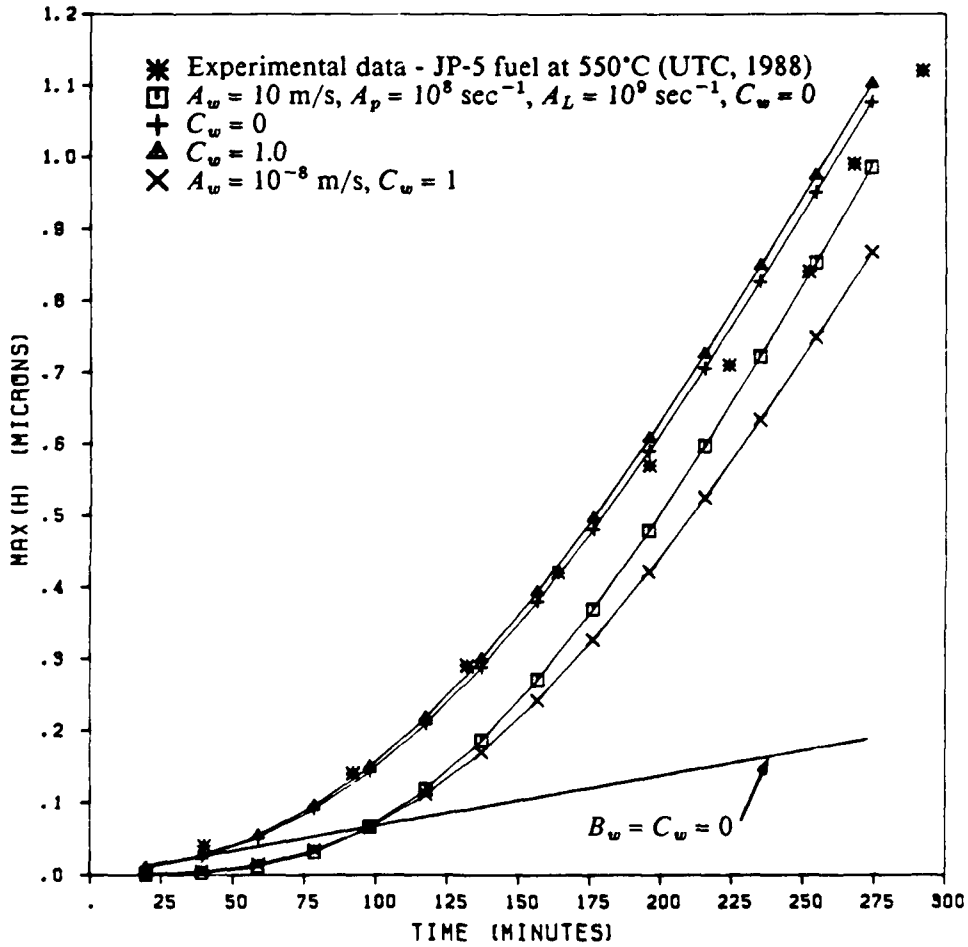


**Figure 5.** **Time-Dependent Growth of the Deposit at Peak Temperature Location for Various Models.** Jet fuel is NACP FF-8 (JP-5); peak experimental temperature is 550°F (286°C). Model activation energies: $E_w$ = 39 kcal/mole, $E_p$ = 30 kcal/mole, $E_L$ = 35 kcal/mole. Also, unless otherwise noted in the figure, $A_w$ = $10^4$ m/s, $A_p$ = $9 \times 10^7$ sec$^{-1}$, $A_L$ = $9 \times 10^8$ sec$^{-1}$, $B_w$ = 1.

Figure 6a shows the axial variation of the solid deposit distribution for various times for a particular calibration study. The rapid nonlinear growth of the deposit with increase in time can be seen in this figure. Figure 6b shows solid deposit distribution at the last time on which the wall temperature is also plotted. The deposit thickness increases with increasing temperature, with the maximum deposition occurring near the peak temperature on the wall.

Figure 7a shows the growth of the liquid precursor (by mass fraction $Y$) near the edge of the solid deposit (at $r = r_2$) for a representative case. It can be seen that peak production of the liquid deposit precursor also occurs in the region where the temperature is high. As time increases, however, the deposit precursor distribution near the rod surface becomes more uniform in the axial direction. In the radial direction, the temperature drops rapidly and the net liquid deposit precursor production also drops rapidly.

Figure 7b shows the axial variation of the temperature of the bulk fuel adjacent to the solid deposit during the calculation for a case with the first two mechanisms of deposit growth [Equation (68)]. As noted in the formulation, we allowed the temperature of the wall and the bulk fuel to adjust to the growth effects of the deposit by virtue of the boundary matching described in Section 3.2. Since we had assumed the thermal conductivity of the deposit to be five times smaller than that of the fuel (i.e., $A_d = 0.2$), this boundary matching results in an increase in the wall temperature with time as the deposit grows and a corresponding decrease in the bulk fuel temperature with growth in the deposit. This is due to the inhibiting effect of the growing deposit layer on the heat transfer process. Figure 7b shows that as the deposit grows, the temperature of the bulk fuel starts to decrease, especially in the regions where the deposit is maximum. As modeled here, this phenomena appears to agree with the observations of Marteney (1988). The wall temperature also begins to increase; however, the effect of the solid deposit on the temperature is not very significant in the range of growth modeled here. Therefore, as a first approximation, we could have neglected this effect and assumed that the deposit growth does not affect the heat transfer between the heated surface and the fuel. Additional study using different values for the thermal conductivity (for example, $A_d = 0.02$) showed that in this case the effect of deposit growth on the heat transfer process could be substantial. The significance of this mechanism can only be quantified if the physical properties, such as the dependence of the deposit thermal conductivity on temperature, $\kappa_d(T)$, are known.

This validation study did, however, allow us to calibrate the model for the nonlinear variation observed in the JFTOT. Subsequent to this study (near the end of Phase I), we obtained the data of Marteney and Spadaccini (1986) and the computed calibration by Krazinski et al. (1990). This data was obtained using a different test apparatus and included data on deposit growth which showed that the wall activation energy was probably much lower than that estimated from the JFTOT data. A choice of $E_w = 8$ kcal/mole was considered more appropriate. Since this was quite different from the earlier choice of $E_w = 39$ kcal/mole used in our calibration study described above, we decided to study the effect of changing the wall activation energy.

Note that our model had two primary mechanisms, the wall catalytic reaction and the nonlinear growth due to the bulk fuel precursor undergoing phase transition and impacting in a random sense on the wall. Thus, if our model was formulated correctly, and if the wall activation energy $E_w$ was reduced to 8 kcal/mole, then the only calibration that should be required is to determine the new value of $A_w$ with $B_w = 0$ and $C_w = 0$. Then if the new calibrated wall catalytic reaction mechanism is combined with the model for the bulk fuel phase change calibrated earlier, the predicted growth of the deposit with time should still agree with the experimentally observed variation. This was in fact observed in our study as shown below.

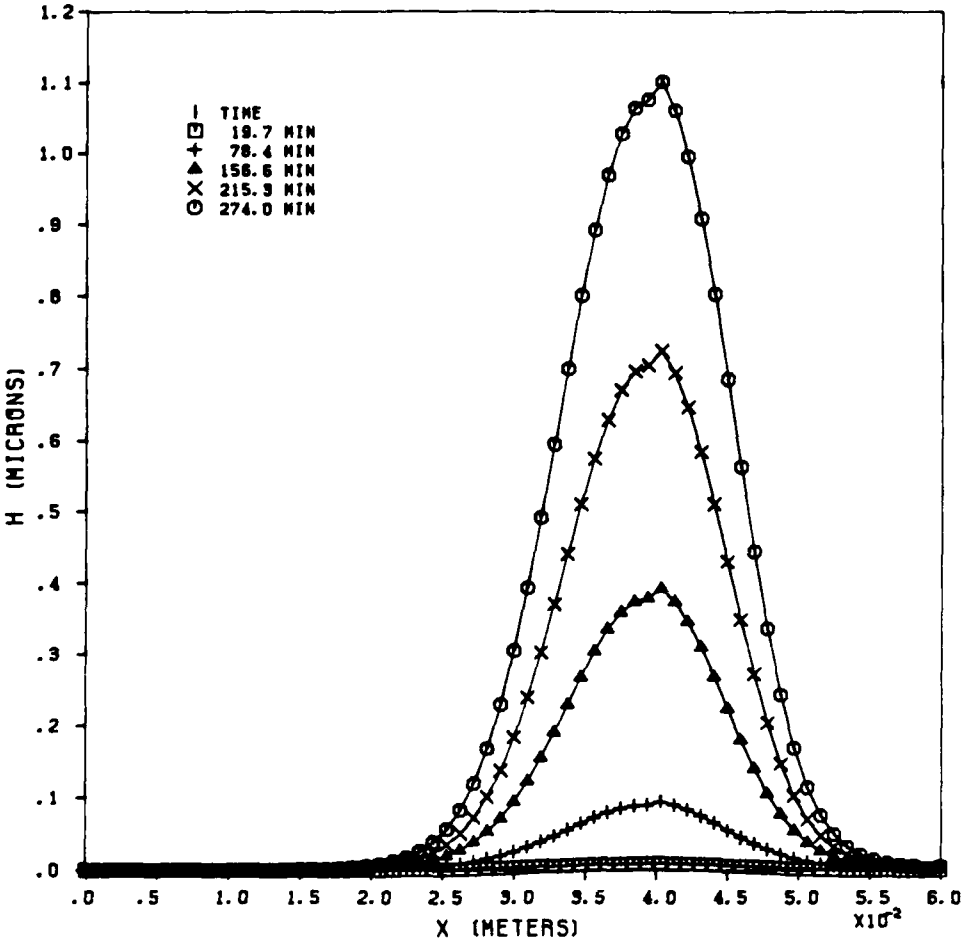


a. As a function of time

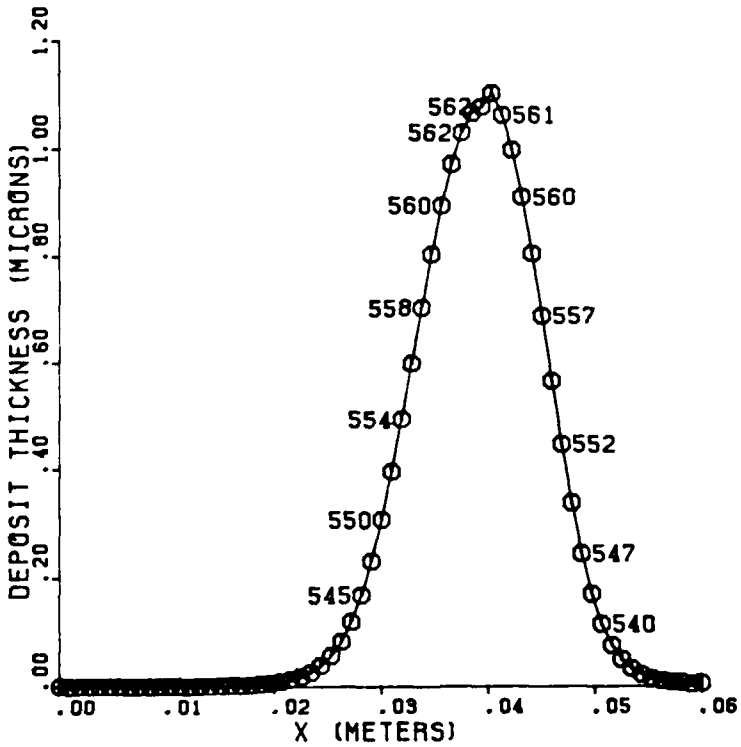


b. After approximately 4.5 hours (numbers on curve indicate wall temperature)

**Figure 6.** **Axial Variation of the Deposit Thickness on the Rod Surface.** Test conditions: $E_w$ = 39 kcal/mole, $E_p$ = 30 kcal/mole, $E_L$ = 35 kcal/mole, $A_w$ = $10^4$ m/s, $A_D$ = $9\times10^7$ sec$^{-1}$, $A_L$ = $9\times10^8$ sec$^{-1}$, $C_w$ = 1, $B_w$ = 1.

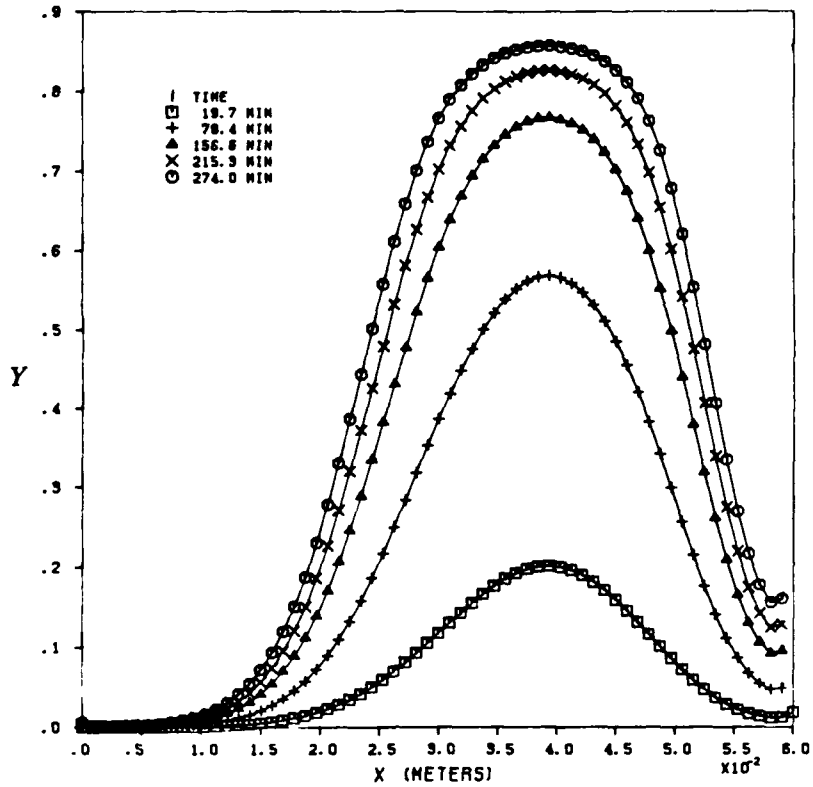


a. Deposit precursor in the bulk fuel near the solid deposit surface as a function of time

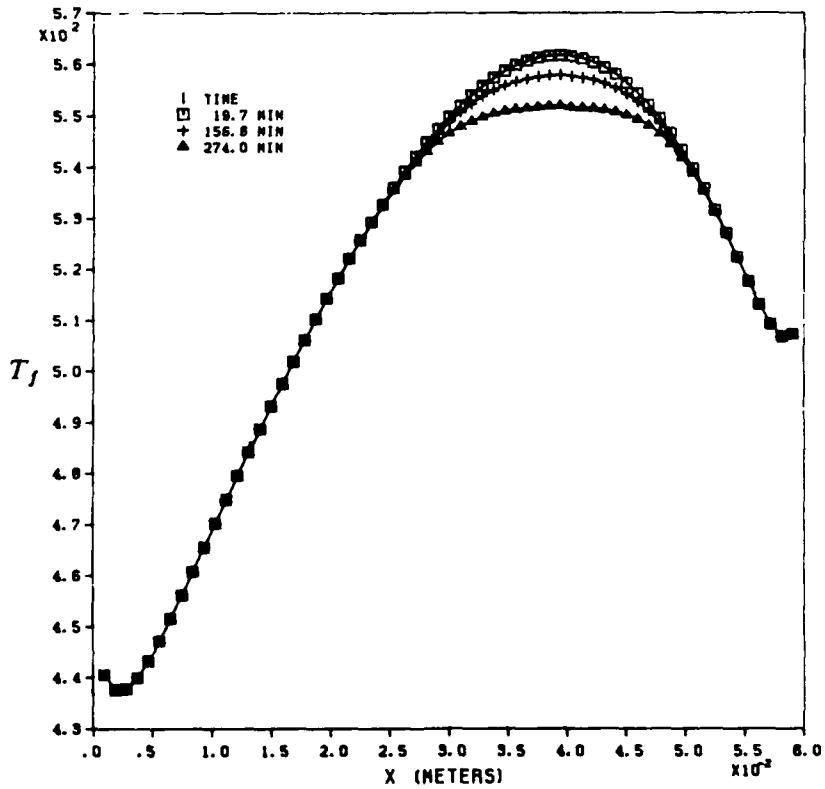


b. Fuel temperature next to the solid deposit surface as a function of time

**Figure 7.** **Axial Variation of the Deposit Precursor and the Fuel Temperature.** Test conditions same as in Fig. 6.

Figure 8 shows the time growth of the deposit on the wall using the new calibration for the wall activation energy of $E_w$ = 8 kcal/mole. As expected, once the linear growth model for the wall catalytic conversion was modeled (i.e., $A_w$ was determined), the combined model again predicts the same nonlinear growth. This appears to indicate that the proposed nonlinear mechanism may have some real validity. Of course, the validity of the model can only be confirmed if additional experimental data is obtained to determine the proposed $\sqrt{h}$ variation for the growth of the deposit thickness with time does in fact occur in the actual experiments. Future experiments could be designed to determine if the mechanism proposed in this model is correct.

Figures 9a and 9b show the axial growth of the deposit with time for the cases in which the third mechanism was neglected and for the case in which the modified form of the third mechanism [Equation (81)] was included, respectively. Comparison shows that for the case in which the third mechanism was neglected, the axial distribution is quite smooth. However, with the modified mechanism, the axial growth of the deposit downstream of the peak temperature location is higher. This trend appears to be similar to the increase in the deposit thickness downstream of the peak temperature observed in the JFTOT data (UTC, 1988). In Figure 9c, the temperature is plotted on the curve for the axial variation of the deposit growth at the end of the calculation in which the third mechanism was included. For the same wall temperature, the thickness of the deposit downstream of the peak temperature is larger when compared to the upstream value.

## 6. CONCLUSIONS AND RECOMMENDATIONS

In this Phase I study, a detailed mathematical model was developed that would allow the modeling of the various possible physical mechanisms that lead to the thermal degradation of jet fuels and the subsequent formation of solid deposits on a heated surface. The mathematical formulation would allow the calculation of the heat conduction through the heated metal surface, the heat transfer through the solid deposit, the conservation of mass momentum and energy in the bulk fuel, the chemical kinetic processes in the bulk fuel, and the time-dependent mechanism for the growth of the solid deposit on the wall. In general, the model developed is applicable to three-dimensional flows of fuels in appropriate fuel systems. If a turbulence model is included, then turbulent flows can also be studied. Time- and space-accurate numerical schemes, both explicit and implicit, were developed for use with this model in this study.

Although the mathematical model formulated was quite general, it was not possible to solve the complex mathematical equations for a multispecies two-phase flow in Phase I. Therefore, a simplified model was reduced from the general formulation using axisymmetric assumptions and then solved using the numerical scheme developed in this study. The steady-state temperature distribution in the heating element and in the bulk fuel was calculated using this numerical scheme. It was demonstrated that under the axisymmetric approximation, the temperature distribution will not agree with the observed JFTOT variation if the constant heat flux boundary condition is used. By modifying the heat flux distribution, however, we were able to reproduce the JFTOT variation. Since this was as good as using the curve fits for the experimental data, we used the curve fits to obtain the steady-state temperature field in the bulk fuel for the calibration studies.

With the computed temperature field, we carried out a series of calibration studies to obtain the calibration constants for the deposit growth and the liquid precursor. These studies showed that the proposed growth mechanism could be made to agree with the JFTOT experimental data on the nonlinear growth rate (UTC, 1988) quite well. This appears to indicate that the proposed mechanism may have some validity.

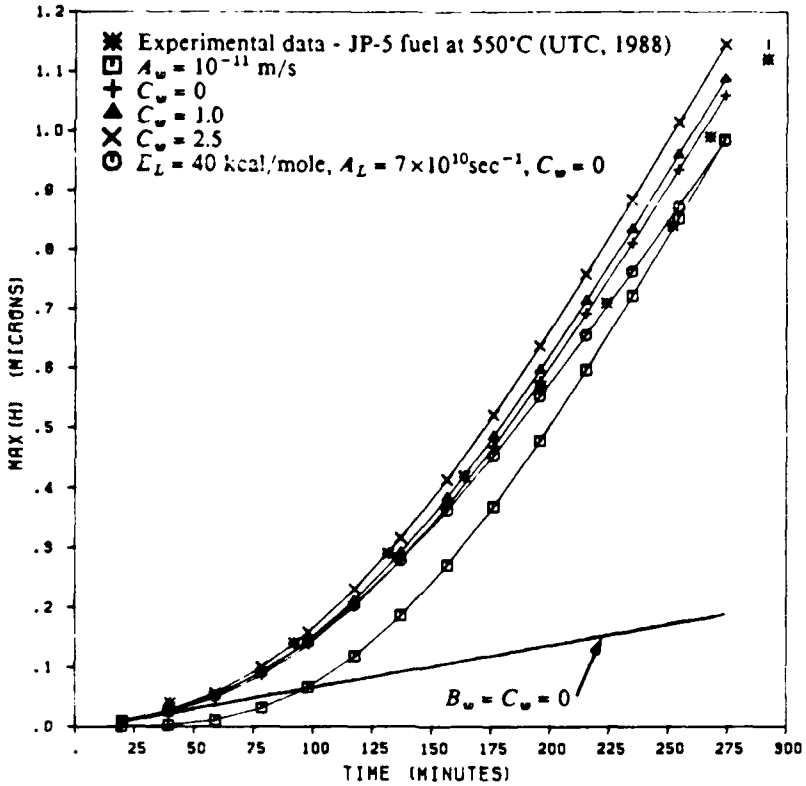


**Figure 8.** **Time-Dependent Growth of Deposit Thickness at the Peak Temperature Location for $E_w$ = 8 Kcal/mole.** Jet fuel and peak experimental temperature same as in Fig. 5. Also, unless otherwise noted in the figure, $E_p$ = 30 kcal/mole, $E_L$ = 35 kcal/mole, $A_w = 8\times10^{-9}$ m/s, $A_p = 9\times10^{7}$sec$^{-1}$, $A_L = 9\times10^{8}$sec$^{-1}$, $B_w$ = 1, $C_w$ = 0.

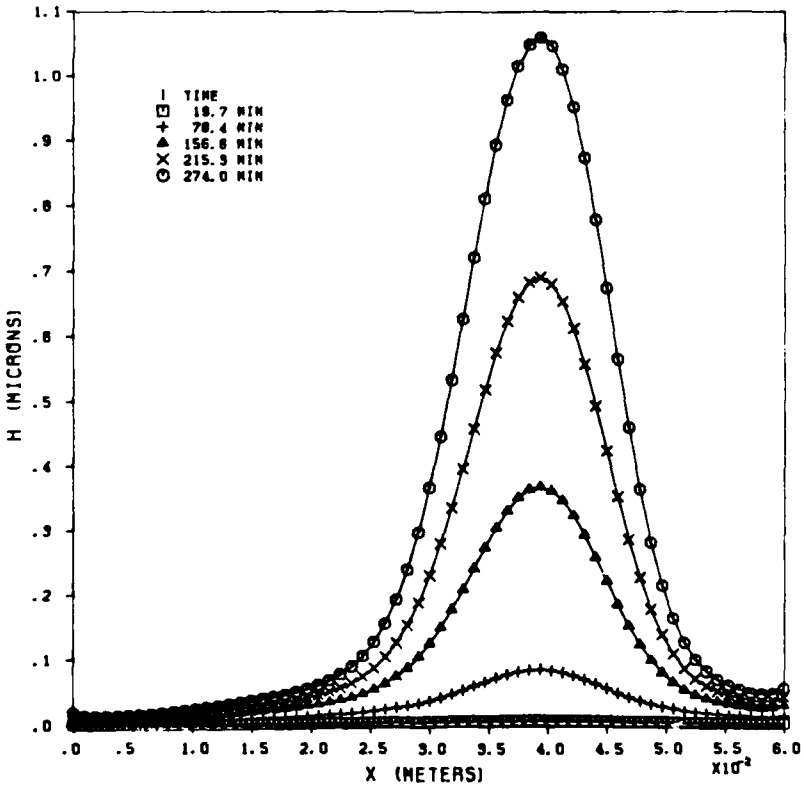


**a. As a function of time.** Test conditions: $E_w$ = 8 kcal/mole, $E_p$ = 30 kcal/mole, $E_L$ = 35 kcal/mole, $A_w = 8\times10^{-9}$ m/s, $A_p = 9\times10^{7}$ sec$^{-1}$, $A_L = 9\times10^{8}$ sec$^{-1}$, $B_w$ = 1, $C_w$ = 1.

**Figure 9.** **Axial Variation of Deposit Thickness**

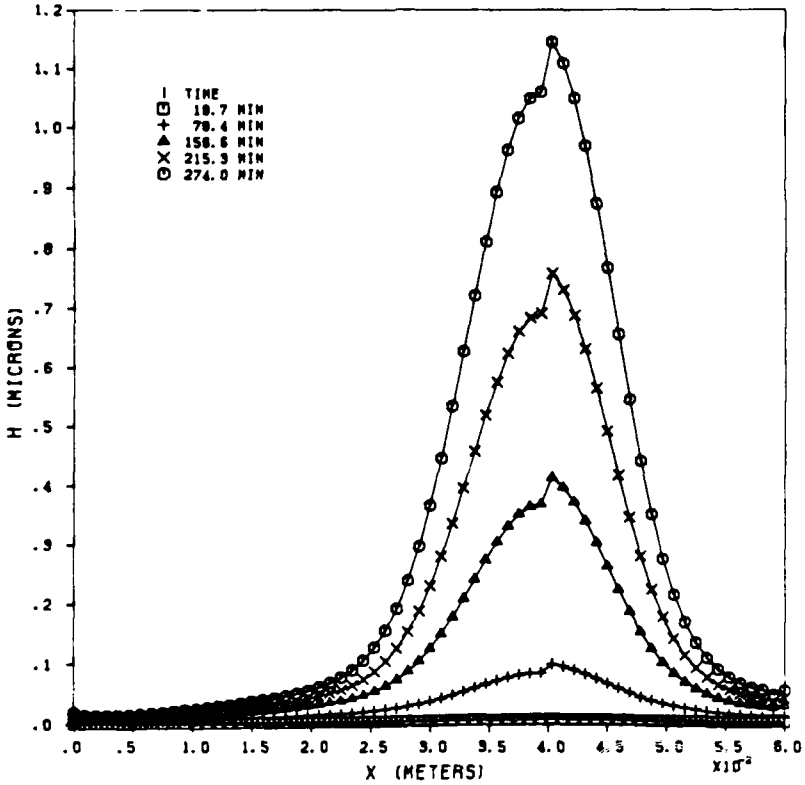


**b. As a function of time.** Test conditions same as in Fig. 9a except $C_w = 2.5$.

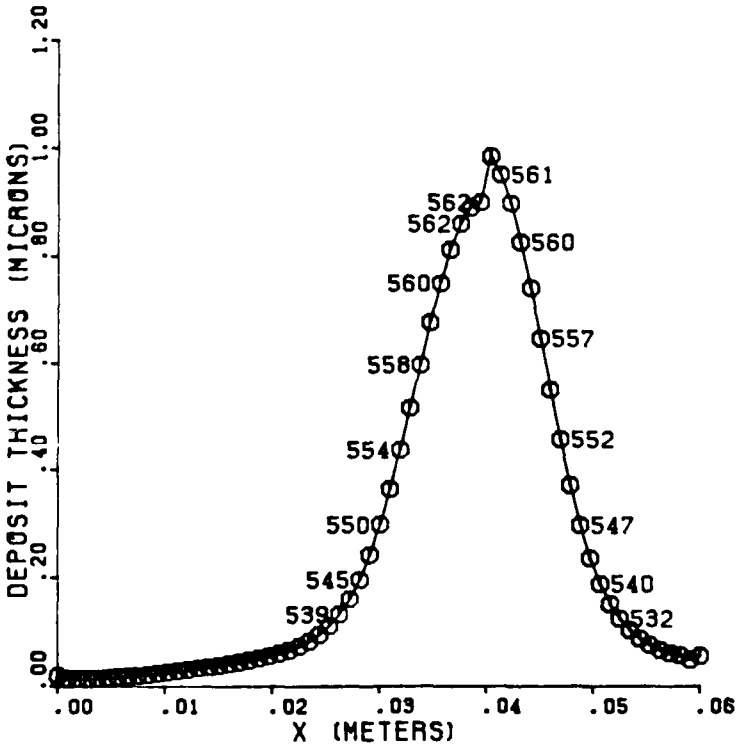


**c. After approximately 4.5 hours (numbers on curve indicate wall temperature).** Test conditions same as in Fig. 9b.

**Figure 9. Axial Variation of Deposit Thickness (Cont.)**

One of the major hurdles facing the validation of CFD models such as the one developed here to study the thermal degradation process is that many of the mechanisms leading to the growth of the solid deposit are largely unknown. In addition, the experimental data available are quite limited both in quality and quantity. In the present study, we used primarily one set of data based on the JFTOT experiments to calibrate our model. The reduced model used in Phase I appears to show good agreement with the experimental data of the JFTOT study (UTC, 1988). However, it is not clear if the JFTOT data itself is an accurate representation of the actual thermal degradation process. In addition, the data makes no attempt to quantify the physical process leading to deposit growth and provides only gross information on the amount of deposit on the heated surface. Thus, although the model appears to be validated by comparison with the data, it is not clear if the physical mechanism proposed for the growth of the deposit is a valid representation of the actual physics of the complex chemical processes involved in the thermal degradation of the jet fuels. Therefore, it is probably premature to further extend this model at this stage to include the two-phase full model formulated in this study. More controlled and detailed experimental studies must be conducted before additional evaluation of CFD models can be carried out. Such experiments can be considered in the next phase so that additional data is available before further model development is carried out.

## REFERENCES


Anderson, D. A., Tannehill, J. C., and Pletcher, R. H. (1984) *Computational Fluid Mechanics*, Hemisphere Publishing Corporation, New York.

Chin, J. C., Lefebvre, A. H., and Sun, F. (1989) "Temperature Effects on Fuel Thermal Stability," Purdue University Report.

Cohen, S. M. (1980) "Fuels Research - Fuel Thermal Stability Overview; Aircraft Research and Technology for Future Fuels," NASA CP-2146, pp. 161-168.

CRC (1978) "Research Technique for Thermal Stability by Modified Jet Fuel Thermal Oxidation Test (JFTOT)," Coordinating Research Council Report No. 496, Coordinating Research Council, Inc., New York, NY, June.

CRC (1979) "CRC Literature Survey in the Thermal Oxidation Stability of Jet Fuels," Coordinating Research Council Report No. 509, Coordinating Research Council, Inc., Boca Raton, Florida, April.

Dahlin, K. E., Daniel, S. R., and Worstell, J. H. (1981) "Deposit Formation in Liquid Fuels. 1. Effect of Coal-Derived Lewis Bases on Storage Stability of Jet A Turbine Fuel," *Fuel*, Vol. 60, No. 6, pp. 477-480.

Daniel, S. R. (1983) "Studies of the Mechanism of Turbine Fuel Instability," Colorado School of Mines, NASA CR-167963.

Daniel, S. R. (1985) "Jet Fuel Instability Mechanism," NASA Final Report, Contract NA6-3-197.

Davies, J. T. (1987) "Aerosol Deposition from Turbulent Fluids," in *Encyclopedia of Fluid Mechanics, Vol. 6*, N. P. Cheremisinoff, Ed., Gulf Publishing Co., Houston, Texas, pp. 1039.

Hemlick, L. S., and Seng, G. T. (1984) "FTIR Analysis of Aviation Fuel Deposits," NASA TM 83773, September.

Kendall, D. R., and Mills, J. S. (1986) "Thermal Stability of Aviation Kerosine: Techniques to Characterize their Oxidation Properties," *Ind. Eng. Chem., Prod. Res. Devel.*, Vol. 25, pp. 360-366.

Landau, L. D., and Lifshitz, E. M. (1987) *Fluid Mechanics (Volume 6 of Course of Theoretical Physics)* (2nd Ed.), Pergamon Press, Oxford, England.

Krazinski, J. L., Vanka, S. P., Pearce, J. A., and Roquemore, W. M. (1990) "A Computational Fluid Dynamics and Chemistry Model for Jet Fuel Thermal Stability," to be presented at 35th ASME Int. Gas Turbine and Aeroengine Congress and Exposition, Brussels, Belgium, June 11-14.

Marteney, P. J. (1988) "Thermal Decomposition of JP-5 in Long Duration Tests," United Technologies Research Center Report No. R88-957403-23, prepared for the U.S. NAVY under Contract No. N00140-83-C-9119.N

Marteney, P. J., and Spadaccini, L. J. (1986) "Thermal Decomposition of Aircraft Fuel," *Journal of Engineering for Gas Turbines and Power*, Vol. 108, pp. 648-653.

Nixon, A. C. (1962) in *Autoxidation and Antioxidants*, Vol. II, W. O. Lundberg, ed., Interscience, New York, N. Y.

Nixon, A. C., and Henderson, H. T. (1966) "Thermal Stability of Endothermic Heat Sink Fuels," *Ind. Eng. Chem., Prod. Res. Devel.*, Vol. 5, pp. 87-92.

Oh, C. H., Merrill, B. J., and Wadkins, R. P. (1989) "Three-Dimensional Analysis on Flow and Temperature Distributions for Aircraft Fuel Thermal Stability," Idaho National Engineering Laboratory Report No. EGG-NERD-8622, prepared for U.S. Dept. of Energy under Contract No. DE-AC07-76ID01570, June.

Pai, S.-I. (1977) *Two-Phase Flows (Vieweg Tracts in Pure and Applied Physics, Vol. 3)*, ed. by K. Oswatitsch, Vieweg, Braunschweig.

Peaceman, D. W., and Rachford, H. H. (1955) "The Numerical Solution of Parabolic and Elliptical Differential Equations," *Journal of the Society for Industrial and Applied Mathematics*, Vol. 3, pp. 28-41.

Polezhaev, V. I. (1967) "Numerical Solution of the System of Two-Dimensional Unsteady Navier-Stokes Equations for a Compressible Gas in a Closed Region," *Fluid Dynamics*, Vol. 2, pp. 70-74.

Roquemore, W. M., Pearce, J. A., Harrison, W. E. III, Krazinski, J. L., and Vanka, S. P. (1989) "Fouling in Jet Fuels: A New Approach," presented at 198th National ACS Meeting, Symposium Structure on Future Jet Fuels II, Miami Beach, FL, September 10-15.

Schenk, L., Johnston, R., and Monita, C. (1971) "Investigation of Effects of Trace Metals on the Thermal Stability of JP-7 Fuels," Air Force Aero Propulsion Lab., Wright Patterson AFB, Ohio, AFAPL-TR-71-98, December.

Taylor, W. F. (1967) "Kinetics of Deposit Formation from Hydrocarbon Fuels at High Temperature: General Features of the Process," *Ind. Eng. Chem., Prod. Res. Devel.*, Vol. 6, pp. 258-262.

Taylor, W. F. (1969a) "Kinetics of Deposit Formation from Hydrocarbons: Fuel Composition Studies," Ind. Eng. Chem., Prod. Res. Devel., Vol. 8, pp. 375-380.

Taylor, W. F. (1969b) "Kinetics of Deposit Formation from Hydrocarbons. IV. Additive and Surface Coating Effects," *J. Appl. Chem.*, Vol. 19, pp. 222-226.

Taylor, W. F. (1970) "Catalysis in Liquid Phase Autoxidation. II. Kinetics of the Poly (tetrafluoroethylene)-Catalyzed Oxidation of Tetralin," *J. Phy. Chem.*, Vol. 74, pp. 2250-2256.

Taylor, W. F. (1974) "Deposit Formation from Deoxygenated Hydrocarbons. I. General Features," *Ind. Eng. Chem., Prod. Res. Devel.*, Vol. 13, pp. 133-138.

Taylor, W. F. (1976) "Deposit Formation from Deoxygenated Hydrocarbons. II. Effects of Trace Sulfur Compounds," *Ind. Eng. Chem., Prod. Res. Devel.*, Vol. 15, pp. 64-68.

Taylor, W. F., and Frankenfeld, J. W. (1978) "Deposit Formation from Deoxygenated Hydrocarbons. III. Effects of Trace Nitrogen and Oxygen Compounds," *Ind. Eng. Chem., Prod. Res. Devel.*, Vol. 17, pp. 86-90.

Taylor, W. F., and Wallace, T. J. (1968) "Kinetics of Deposit Formation from Hydrocarbons: Effects of Trace Sulphur Compounds," *Ind. Eng. Chem., Prod. Res. Devel.*, Vol. 7, pp. 198-202.

UTC (1988) "Properties of Aircraft Fuels and Related Materials," United Technologies Corporation Report No. FR 19032-11, prepared for U.S. Air Force under Contract No. F33615-85-C-2508.